

# Perceptual Video Coding for Machines via Satisfied Machine Ratio Modeling

Qi Zhang, *Student Member, IEEE*, Shanshe Wang, *Member, IEEE*, Xinfeng Zhang, *Senior Member, IEEE*, Chuanmin Jia, *Member, IEEE*, Zhao Wang, *Member, IEEE*, Siwei Ma, *Senior Member, IEEE*, and Wen Gao, *Fellow, IEEE*

**Abstract**—Video Coding for Machines (VCM) aims to compress visual signals for machine analysis. However, existing methods only consider a few machines, neglecting the majority. Moreover, the machine perceptual characteristics are not effectively leveraged, leading to suboptimal compression efficiency. In this paper, we introduce Satisfied Machine Ratio (SMR) to address these issues. SMR statistically measures the quality of compressed images and videos for machines by aggregating satisfaction scores from them. Each score is calculated based on the difference in machine perceptions between original and compressed images. Targeting image classification and object detection tasks, we build two representative machine libraries for SMR annotation and construct a large-scale SMR dataset to facilitate SMR studies. We then propose an SMR prediction model based on the correlation between deep features differences and SMR. Furthermore, we introduce an auxiliary task to increase the prediction accuracy by predicting the SMR difference between two images in different quality levels. Extensive experiments demonstrate that using the SMR models significantly improves compression performance for VCM, and the SMR models generalize well to unseen machines, traditional and neural codecs, and datasets. In summary, SMR enables perceptual coding for machines and advances VCM from specificity to generality. Code is available at <https://github.com/ywwynm/SMR>.

**Index Terms**—Video Coding for Machines, Perceptual Coding, Just Noticeable Difference, Satisfied User Ratio

## 1 INTRODUCTION

INTELLIGENT machines are exploding in recent years. Many machines are designed to analyze and comprehend visual data like images and videos. Over the past decade, by leveraging AI techniques such as convolutional neural network [1], deep learning [2], [3], residual [4] and dense [5] block, knowledge distillation [6], network architecture searching [7], [8], attention mechanism [9], [10], self-supervised learning [11], [12], *etc.*, the capability and efficiency of machine vision systems (MVS) have been rapidly and greatly improved. Nowadays, machines have surpassed humans in several visual analysis tasks [13], [14] and have been widely adopted in various applications.

Like humans seeking high-quality images to satisfy their insatiable visual appetite, machines pursue high-quality visual data for accurate analysis. Such requirement can usually be satisfied during the training phase, where machines learn high-level semantic information from high-quality image datasets, such as ImageNet [15] and Microsoft COCO [16]. However, in the real world, images can be blurred, noisy, in bad luminance, contrast, or low resolution, *etc.*, which increases the difficulty for machines to extract

features with precise semantics and utilize them to perform analysis [17], [18]. Compression artifact might be the most common type of distortion, because images and videos often need to be compressed before spread and used to reduce transmission and storage costs. Several studies [19], [20], [21] have revealed that compression can significantly decrease the analysis accuracy of different models and tasks, compromising the reliability of machines, especially at low bit-rates. Therefore, a great challenge is posed for image and video coding to maintain the effectiveness and robustness of machines in various application scenarios where compression quality levels are varied to meet realistic demands.

In the past decades, image and video coding standards such as JPEG [22], AVC [23], HEVC [24], VVC [25], AV1 [26], and AVS3 [27] have significantly increased compression efficiency. The emerging neural codecs [28], [29] also provide novel and encouraging solutions. However, they are all optimized for human vision systems (HVS) to enhance visual fidelity and quality at similar bit-rates. Recently, several MVS-oriented compression methods have been explored to fill this gap. Some works propose to modify current codecs, such as refining parameter selection [30], [31], rate-distortion optimization [32], [33], [34], and bit allocation [35], [36], [37] modules. Another trend is to learn end-to-end compression networks with machine analysis task-specific constraints [38], [39], [40], [41]. In line with these explorations, the standardization progress has also started by the MPEG organization, namely Video Coding for Machines (VCM) [42], [43], which aims at establishing a promising platform for advancing MVS-oriented coding techniques and further facilitating the deployment of machine vision applications in various domains.

- Corresponding author: Siwei Ma. (Email: [swma@pku.edu.cn](mailto:swma@pku.edu.cn))
- Qi Zhang, Shanshe Wang, Zhao Wang, Siwei Ma, and Wen Gao are with National Engineering Research Center of Visual Technology, School of Computer Science, Peking University, Beijing, China. (Emails: [qizhang@stu.pku.edu.cn](mailto:qizhang@stu.pku.edu.cn), [sswang@pku.edu.cn](mailto:sswang@pku.edu.cn), [zhaowang@pku.edu.cn](mailto:zhaowang@pku.edu.cn), [swma@pku.edu.cn](mailto:swma@pku.edu.cn), [wgao@pku.edu.cn](mailto:wgao@pku.edu.cn))
- Xinfeng Zhang is with University of Chinese Academy of Sciences, Beijing, China. (Email: [xfzhang@ucas.ac.cn](mailto:xfzhang@ucas.ac.cn))
- Chuanmin Jia is with Wangxuan Institute of Computer Technology, Peking University, Beijing, China. (Email: [cmjia@pku.edu.cn](mailto:cmjia@pku.edu.cn))
- Siwei Ma and Wen Gao are also with Peng Cheng Laboratory, Shenzhen, China.

However, existing MVS-oriented compression methods suffer from two notable drawbacks. First, they are usually designed and evaluated with only one or a few specific machines considered, thus lacking generalizability. For example, the common test conditions (CTC) during VCM standardization [44] only involve a single machine to assess the compression quality for the analysis task, introducing inherent bias to the evaluation process and making the results more subjective (accurate and appropriate for that specific machine) than objective (generalized enough for the majority of machines). The potential negative impact from such bias enlarges in the real world when the information of machines used for downstream analysis is unavailable during compression, or when the machines get updated or replaced frequently due to the expeditious evolution of machines as well as the diversity and uncertainty of application requirements. Second, the MVS behaviors are not well exploited and leveraged, especially the machine perceptual characteristics on distinguishing between good and bad compression quality, thus limiting the compression performance. The sub-optimal compression efficiency leads to additional costs in transferring, storing, and processing the input visual data for machines, which becomes increasingly problematic in the age of AI due to the gigantic data volume and ubiquitous applications.

Revisiting traditional HVS-oriented compression methods, perceptual coding is a valuable reference that addresses the aforementioned drawbacks. More specifically, HVS has some intrinsic flaws that can only perceive image content or quality level changes that are larger than a certain threshold [45]. Such characteristics bring in perceptual redundancy in the context of image and video coding, which can be removed during compression. To capitalize on this attribute, the concept of Just Noticeable Difference or Just Noticeable Distortion (JND) is proposed [46] and modeled [47], [48], [49], [50], [51]. JND locates the maximum quality degradation that HVS cannot perceive, thus establishing a theoretically optimal operation point for compression. As visual acuity varies among human individuals, JND is further extended to Satisfied User Ratio (SUR) [52], [53], [54], [55]. SUR is calculated from the cumulative distribution of JND locations obtained from a large population of human subjects, preventing inaccurate or insufficient perceptual characteristics capturing from subject bias. Therefore, SUR can measure image quality in a more generalizable manner. Furthermore, compared with a single JND point, SUR forms a continuous and deterministic model that provides multiple operation points for compression, making it more versatile and applicable.

JND and SUR successfully model the HVS behaviors, enabling the HVS-oriented perceptual coding. More recently, a few works demonstrate the existence of JND for machines [21], [56] and reveal its potential for MVS-oriented perceptual coding. However, unifying the compression generalizability and performance simultaneously for VCM in a practical manner remains an issue of paramount significance. In this work, we make the initial attempt to study SUR for machines to tackle this unprecedented challenge. Our contributions are presented as follows.

- We demonstrate the necessity of involving multiple machines in the VCM progress through two preliminary

experiments. The first one reveals that different machines have distinct perceptions of images in the same compression quality level. The second one indicates that optimizing encoder for one machine may decrease the performance of another.

- We propose a novel concept, Satisfied Machine Ratio (SMR), to model the general MVS characteristics for VCM. SMR is defined as the ratio of machines that exhibit higher satisfaction scores to a certain quality of a compressed image or video frame than a reasonable threshold. Each satisfaction score is calculated based on the differences in machine perceptions of original and compressed images, which reflects the machine's JND profile. To the best of our knowledge, we are the first to explore SUR for machines.
- We make practices for SMR on two fundamental machine visual analysis tasks, image classification and object detection. We build two machine libraries to make statistics on MVS behaviors, comprising up to 72 and 98 representative machine subjects for each task, respectively. Using these machine subjects for SMR annotation, a large-scale SMR dataset containing over 27 million images in 37 compression quality levels and more than 593 million ground truth labels is constructed. This dataset facilitates further SMR studies.
- We analyze the SMR dataset to reveal MVS characteristics individually at the image level and aggregately at the dataset level. We discover a nonlinear negative correlation between deep features differences and SMR. Based on this finding, we propose a full-reference SMR prediction model to predict the SMR of any image or video frame. This model serves as a solid baseline for the SMR prediction and SMR-guided coding optimization task. Furthermore, we introduce an auxiliary task of predicting the SMR difference between a pair of images in different compression quality levels, which leverages all labeled data and helps increasing the SMR prediction accuracy.
- We conduct extensive experiments to verify the proposed SMR models' effectiveness in predicting SMR and improving the compression performance for VCM. Using the predicted SMR as the optimization target of codecs, we achieve a basic BD-rate saving of 28.6%. More importantly, the results remain consistent across different machines, traditional and neural codecs, and unseen datasets, demonstrating the strong generalizability of our SMR models. The evaluations also establish a reliable benchmark for future works on this topic.

In conclusion, SMR enables perceptual coding for machines and advances VCM from specificity to generality. Furthermore, the idea and method of considering the majority of machines instead of one or a few specific machines can benefit other machine vision and image processing areas, including image and video quality assessment and enhancement, adversarial attack, privacy-protected visual analysis, and more.

The rest of our paper is organized as follows. Section 2 presents several related works, including VCM as well as HVS- and MVS-oriented perceptual coding. Section 3 reveals the diversity of machines and its potential negative

impact on existing codecs. In section 4, the concept of SMR is proposed and defined in detail. Subsequently, focusing on image classification and object detection tasks, we construct two machine libraries to obtain the ground truth SMR, and build a large-scale SMR dataset in section 5. In section 6, a deep learning-based SMR model is proposed for SMR prediction. Section 7 shows the experimental results of evaluating the SMR model's performance, particularly in increasing the coding efficiency for machines and its generalizability. Finally, section 8 concludes the paper.

## 2 RELATED WORKS

### 2.1 Video Coding for Machines

VCM aims at compressing visual signals efficiently while keeping their utility for machine analysis. Several works are proposed to improve the coding performance for MVS in multiple ways [57]. The first is to optimize conventional image and video codecs for MVS. Liu *et al.* [30] trained a support vector machine (SVM) to predict whether the image quality is good enough for correct machine analysis by the differences of SIFT features before and after compression. The prediction is then used for choosing adequate coding configurations for MVS. Shi *et al.* [58] and Li *et al.* [31] adopted deep reinforcement learning technique to select quantization parameters for coding tree units (CTU) in HEVC, where the reward function is related to both bit-rate and machine analysis accuracy. Li *et al.* [59] and Zhang *et al.* [33] introduced task-specific quality metric in the rate-distortion optimization (RDO) procedure of HEVC to obtain better analysis results under the same compression rate. In [36], a bit allocation strategy is designed to assign more bits to regions with higher activations from shallow task network layers. Similarly, Huang *et al.* [37] proposed a multi-scale feature distortion metric for RDO with salient areas detected by a pre-trained region proposal network.

The second way is to train an end-to-end neural codec for MVS. In [38], two types of deep semantic image coding frameworks were proposed, distinguished by analysis being performed on encoder or decoder side. The codec combined bit-rate, signal-level, and task-level errors to form the training loss function. Torfason *et al.* [39] trained a network for both compression and analysis, where the compact representation generated by the codec is directly used for analysis without reconstructing image textures. Codevilla *et al.* [60] and Chamain *et al.* [61] attached various task networks to produce different losses for optimizing the codec and improving its generalizability. To further increase the coding efficiency, state-of-the-art AI techniques like vision transformers [40] and contrastive learning [62] are introduced. More recently, scalable layered coding becomes a trending compression framework for both humans and machines. Akbari *et al.* [63] proposed to include a semantic segmentation map as the base layer, which is compressed losslessly for analysis tasks. Their framework also contains a primary enhancement layer where textures are generated by a decoder network, and the residual between the original image and generated one is also compressed as the secondary enhancement layer. The segmentation map was replaced by an edge map in [64], [65], [66], [67] or deep features in [68], [69]. Yan *et al.* [70] performed layered coding to features,

where features from different layers of the network have distinct semantic granularities for multiple analysis tasks and texture reconstruction as well [71]. Similarly, Liu *et al.* [72] designed a transformation network based on a lifting scheme to convert images into multi-level scalable representations and compress them in an end-to-end manner. Tu *et al.* [73] utilized the correlation between neighboring network layers and the different importance between object and background areas to improve compression performance. Choi *et al.* [74] purposefully split the latent representations into two parts during training, where the first part stores semantics for analysis as the base layer and the second stores textures information for reconstruction as the enhancement layer. The generated scalable bit-stream can be arranged structurally, where different parts of the bit-stream stores information from different layers [75], [76], [77], [78] to support on-demand transmission and storage.

Many efforts are also made from standardization perspective. As early as in the late 1990s, MPEG has explored the content description of images and videos for intelligent identification, categorization, and user-browsing, from which the international MPEG-7 visual standard was born [79]. In 2015, the Compact Descriptor for Visual Search (CDVS) standard [80] was declared, which defines the bit-stream of descriptors (*i.e.* hand-crafted visual features) and the descriptor extraction process for image matching and retrieval task. Its successor, the Compact Descriptor for Video Analysis (CDVA) [81], was finalized in 2019, which introduces deep features and enables machine analysis on videos. These former standards promote the standardization of Digital Retina [82] in China, which consists of three bit-streams (videos, features, and models) to support applications at scale. Meanwhile, internationally, MPEG began to develop the Video Coding for Machines standard [43], pursuing high-efficiency visual signal compression, better machine analysis performance, computational offloading, and privacy preserving at the same time.

Although there is significant progress in VCM, existing methods have the two drawbacks mentioned in section 1. In this paper, we will address these issues to improve VCM for satisfying the compression needs of different machines efficiently.

### 2.2 Perceptual Coding for Humans

HVS cannot perceive tiny distortions caused by image and video coding. JND models take advantage of this behavior to determine an optimal operation point for compression that balances bit-rate and perceptual quality. To study JND, researchers have created several image and video databases such as MCL-JCI [83], MCL-JCV [84], and VideoSet [52]. Utilizing these datasets, JND can be modeled in different granularities like pixel, sub-band, and picture or video wise [45], [85]. Picture or video wise JND is more reasonable because HVS perceives image/video entirely instead of pixel or sub-band individually, and is also more applicable because it can be achieved more easily by adjusting coding parameters. Huang *et al.* [86] predicted JND with a support vector regressor (SVR) using hand-crafted spatio-temporal features. Liu *et al.* [49] developed a deep learning-based JND estimation framework, converting the task into a binary

classification problem to predict whether two images are perceptually identical, then JND can be searched. Tian *et al.* [87] trained a CNN to predict the JND of a distorted image without the original image as reference, and also used an SVR to predict the number of JND levels. In [50], the structural visibility was firstly predicted at the image-patch level, and then the image-level JND can be estimated by collecting results from all patches. Since humans are different, JND is extended to SUR to represent the HVS characteristics of many human subjects. Wang *et al.* [88] predicted SUR with quality degradation and temporal masking features, which can also be used to locate JND points [89]. Fan *et al.* [53] designed a Siamese CNN with shared weights to predict SUR based on transfer learning. The network architecture is optimized in [90] by fusing features from different layers to decrease the SUR estimation error. Zhang *et al.* [54] combined saliency distribution, masking effect, quality degradation, and bit-rate change features to train an SVR for predicting SUR. In [55], a two-stream CNN was developed to predict video-wise SUR using spatio-temporal features, which are fused at the quality score and feature levels. Due to the differences in principle and target between HVS and MVS, existing perceptual coding methods for humans cannot be directly applied for machines, which will be studied extensively in this work.

### 2.3 Perceptual Coding for Machines

It is still at an early age for perceptual coding for machines. There are a few works exploring the JND profile of MVS. Zhang *et al.* [21] proposed the concept of Just Recognizable Distortion (JRD), which presents the maximum compression distortion that will not cause machine recognition failure. They built a large JRD dataset where JRD is measured by the quantization parameter used for coding, and developed an ensemble learning-based JRD prediction framework for multiple analysis tasks, which can increase the task performance under the same bit-rate. Jin *et al.* [56] demonstrated the existence of JND for image classification task, and proposed a generative model to predict pixel-level JND map and create a JND image. According to their experiments, machines can tolerate the JND image with an average peak signal-to-noise ratio (PSNR) of only 9.56dB, which defines a boundary for lossy compression to realize lossless machine analysis. However, these works did not consider the diversity of machines thoroughly and had some other problems. In [21], the JRD of four machines for two analysis tasks are studied individually. In [56], only four old-fashioned machines for the single image classification task are considered together, and the JND model cannot be directly used in VCM codecs. In this work, we will further improve the generalizability for perceptual coding for machines in a practical manner.

### 3 DIVERSITY OF MACHINES

We first study the diversity of machines in the context of image and video coding through two experiments. We meticulously collect 12 different machines for these experiments, which are VGG-19 [2], ResNet-50, ResNet-101 [4], ResNeXt-101 [91], DenseNet-161 [5], MobileNet-v3-Large [92], EfficientNet-B0, EfficientNet-B4 [93], Vision

Transformer-B/16 [9], ConvNeXt-Base [94], Swin-T, and Swin-B [10]. Despite the differences in macro architectures (e.g. CNNs *vs.* transformers), these machines also differ in internal modules (VGG *vs.* DenseNet), size (MobileNet *vs.* the others), depth (ResNet-50 *vs.* ResNet-101), overall scale (EfficientNet-B0 *vs.* EfficientNet-B4), and "modernization" [94] (ResNet-50 *vs.* ConvNeXt-Base). Therefore, a comprehensive examination can be conducted to explore the potential similarities and dissimilarities among these machines.

**In the first experiment, we demonstrate that different machines have distinct MVS characteristics by comparing their perceptions under the same compression quality level.** To generate the necessary input data for machines, we encode images from the val2017 dataset of MS COCO [16] with HM-16.24, the reference software of HEVC. Each image is compressed as an intra video frame, where various quality levels are produced by altering the quantization parameter (QP) during the compression process. Specifically, 20 QPs are selected, which are 32, 33, . . . , and 51, where a larger QP leads to worse reconstruction quality. It should be mentioned that we employ relatively large QPs in this experiment because typically smaller QPs only result in tiny distortions that are negligible for MVS [19], [21].

We randomly crop 10,000 objects from COCO images with ground truth bounding boxes to recognize their categories using selected machines. The initial weights of all machines are from PyTorch [95], which are trained on the ImageNet, and we fine-tune them on the original COCO train2017 dataset using object images to adapt to COCO semantics. Since machines are created to analyze and understand image content, their perceptions are equivalent to analysis results. Therefore, we record the top-1 predictions (*i.e.* the category of the largest probability) from  $m$ th machine  $M_m$  on  $i$ th object image  $I_i$  across 21 quality levels, *i.e.* compressed by 20 QPs plus the uncompressed one, namely  $I_i^{32}, I_i^{33}, \dots, I_i^{51}$ , and  $I_i^0$ . The predictions are denoted as  $M_m(I_i^{32}), M_m(I_i^{33}), \dots, M_m(I_i^{51})$ , and  $M_m(I_i^0)$ . Subsequently, we compute a **machine perception consistency label** for the prediction of  $M_m$  to  $I_i$  in compression quality level  $QP_k$  using the following formulation:

$$L(M_m; I_i^{QP_k}) = \begin{cases} 1, & \text{if } M_m(I_i^{QP_k}) = M_m(I_i^0) \\ 0, & \text{otherwise} \end{cases}. \quad (1)$$

When the label is 1, the machine's perception or the compressed image is identical to that of uncompressed, suggesting that the machine is not affected significantly. Otherwise, the compression has a substantial impact on the machine. For machine  $M_m$ , we can generate a **machine perception consistency sequence** of such labels to object image  $I_i$  across all compression quality levels, which is denoted as

$$\text{Seq}(M_m; I_i) = [L(M_m; I_i^{32}), L(M_m; I_i^{33}), \dots, L(M_m; I_i^{51})]. \quad (2)$$

Finally, we calculate the **diversity score** for a pair of machines  $M_m, M_n$  to object image  $I_i$  by

$$S_{\text{div}} = \text{HD}(\text{Seq}(M_m; I_i), \text{Seq}(M_n; I_i)), \quad (3)$$

where  $\text{HD}(\cdot)$  returns the Hamming distance of two sequences. Therefore, a high diversity score between two

machines means that their perceptions are significantly different on the same compression levels of an image.

TABLE 1

The diversity scores of pairs of machines measured by the average Hamming distance of machine perception consistency sequences on 10,000 original and compressed images. Numbers on the first row/column are indices of the selected 12 machines.

	1	2	3	4	5	6	7	8	9	10	11	12
1	0											
2	3.98	0										
3	4.08	3.62	0									
4	4.16	3.69	3.59	0								
5	4.21	3.74	3.77	3.66	0							
6	3.93	3.87	3.85	3.93	3.95	0						
7	3.97	3.89	3.85	3.89	3.92	3.33	0					
8	4.30	4.21	4.14	4.22	4.29	3.91	3.86	0				
9	4.28	3.99	3.83	3.80	3.95	3.81	3.87	4.21	0			
10	3.91	3.58	3.48	3.47	3.54	3.53	3.54	3.84	3.41	0		
11	3.95	3.71	3.62	3.59	3.71	3.56	3.57	4.02	3.31	3.10	0	
12	4.01	3.70	3.58	3.55	3.73	3.53	3.59	4.00	3.18	2.97	2.65	0

The diversity scores of the collected machines in pairs are presented in TABLE 1, where the results are averaged from 10,000 object images for three times. For each time, the objects are re-selected. The numbers shown on the first row/column correspond to the indices of different machines, which are maintained in the same order as their appearance in the first paragraph of this section. Considering all machine pairs, the average overall diversity score is 3.76, meaning that machines’ analysis results differ in 18.8% of all 20 compression quality levels. Examining specific machine pairs, there are no unexpected or significant outliers. The machine pairs with the three highest diversity scores are VGG-19 and EfficientNet-B4, DenseNet-161 and EfficientNet-B4, and VGG-19 and Vision Transformer-B/16, respectively. And the machine pairs with the three lowest diversity scores are Swin-T and Swin-B, ConvNeXt-Base and Swin-B, and ConvNeXt-Base and Swin-T, respectively. In general, the diversity of machines is consistently non-negligible, especially when machines with the same architecture but differing in only depth or overall scale can still yield high diversity scores, such as ResNet-50 and ResNet-101 or EfficientNet-B0 and EfficientNet-B4.

How does such diversity influence VCM? **We prove that a VCM codec optimized for one machine may be ineffective or even lead to worse performance for another.** In this experiment, we treat the codec as a black box, randomly modify the coding configuration, and investigate whether these modifications bring consistent changes to machine perceptions across different machines. More specifically, for object image  $I_i$ , we first randomly select a QP in [32, 51], namely  $QP_{base}$ , and obtain the machine perception consistency label  $L_m^{base} = L(M_m; I_i^{QP_{base}})$  for machine  $M_m$ . Next, we simulate modifying the codec by randomly adding or subtracting a value in the range of [1, 5] from  $QP_{base}$ , resulting in a modified QP as  $QP_{mod}$ , and record the new label  $L_m^{mod}$  after the modification. Note that the modified QP will be adjusted to [32, 51] if it exceeds the QP boundary, and it is ensured that  $QP_{mod} \neq QP_{base}$ . Finally, we compare the changes of labels of a pair of machines  $(M_m, M_n)$ , which are  $\Delta L_{M_m} = L_m^{mod} - L_m^{base}$  and  $\Delta L_{M_n} = L_n^{mod} - L_n^{base}$ . We describe the modification as non-ideal if:

- $\Delta L_{M_m} \neq \Delta L_{M_n}$  and  $\Delta L_{M_m} = -1 \vee \Delta L_{M_n} = -1$ ,

because the perception of one machine deteriorates to be inconsistent with the original image while another gets improved or at least remains the same. Hence, the optimization to VCM codec for one machine leads to worse performance for another.

- $\Delta L_{M_m} \neq \Delta L_{M_n}$  and  $\Delta L_{M_m} \neq -1 \wedge \Delta L_{M_n} \neq -1$  and  $L_m^{base} = L_m^{mod} = 0 \vee L_n^{base} = L_n^{mod} = 0$ , because the perception of one machine gets improved to be consistent with the original image while another still remains inconsistent. Hence, the optimization to VCM codec for one machine is ineffective for another.

To make the investigation more reliable, we also randomly select 10,000 object images for machine analysis and repeat the experiment three times. The same 12 machines collected for the first experiment are still used in this one. The pair of machines for comparison is also generated randomly for each object image. According to the result, averagely, 13.46% of all codec modifications are non-ideal. Therefore, the diversity of machines should not be ignored in the VCM progress.

#### 4 SATISFIED MACHINE RATIO

To properly consider the diversity of machines for VCM and enable MVS-oriented perceptual coding, we propose the concept of *SMR*. The definition of SMR of an image or video frame is given as follows. Let  $I_0$  be the original image that is compressed into several distorted variants  $I_{q_1}, I_{q_2}, \dots, I_{q_n}$ , where  $q_i$  denotes a certain quality level that deteriorates as  $i$  increases. Each machine  $M_j$  in the infinite set  $\mathbb{M}$  containing all machines has a *satisfaction score* to  $I_{q_i}$ , which is denoted by  $S(M_j; I_{q_i})$  and will be described in detail soon. Then, the SMR of  $I_{q_i}$  is calculated as

$$SMR(I_{q_i}) = \frac{|\{M_j \mid S(M_j; I_{q_i}) \geq T_S\}|}{|\mathbb{M}|}, \quad (4)$$

where  $T_S$  is a threshold value for satisfaction score, and  $|\cdot|$  counts the number of elements in the set. As such, SMR statistically represents the proportion of machines satisfied with a certain level of image compression quality. During the SMR calculation,  $T_S$  controls the strictness of how machine perception consistency is judged, which is customizable. A large  $T_S$  indicates that the machine is satisfied with the compression quality only when its perception is very similar between the original and compressed image, which usually means a high analysis accuracy. And a smaller  $T_S$  allows for a more noticeable variation between machine perception of the original and compressed image.

The computation of satisfaction scores varies for different machine analysis tasks because they have distinct objectives and measurements. In this work, we study SMR for two fundamental tasks, image classification and object detection. For the image classification task, we determine the satisfaction score function in a similar form as Eq. (1) in section 3, but extend it for more flexibility:

$$S(M_j; I_{q_i}) = \begin{cases} 1, & \text{if Top-1}(M_j(I_{q_i})) \subseteq \text{Top-K}(M_j(I_0)) \\ 0, & \text{otherwise} \end{cases}, \quad (5)$$

where  $M_j(I_{q_i})$  is the output probabilities for each category from  $M_j$  given  $I_{q_i}$  as input, and  $\text{Top-1}(\cdot)$  and  $\text{Top-K}(\cdot)$  return the set of category indices with top-1 and top-K probability value(s), respectively. When calculating the final SMR for the image classification task using Eq. (4),  $T_S$  can be set to any negative number. Therefore, SMR for this task represents the proportion of machines with similar category predictions on original and compressed images.

The satisfaction score function for object detection is more complicated. There are several factors for evaluating the performance of a detector, such as the intersection over union (IOU) between the detected bounding box and ground truth, the class confidence of an object, and the number of detections that are allowed for the evaluation. The mean average precision (mAP) is the *de facto* metric for this task that considers these factors. By introducing the mAP metric, we determine the satisfaction score function for object detection as

$$S(M_j; I_{q_i}) = \text{mAP}_{T_{\text{IOU}}}(M_j(I_{q_i}), \mathcal{F}_{T_{\text{conf}}}(M_j(I_0))), \quad (6)$$

where  $T_{\text{IOU}}$  is the threshold value of IOU when calculating mAP, and  $\mathcal{F}_{T_{\text{conf}}}(\cdot)$  is a filter function that returns a set of detections that have higher class confidences than  $T_{\text{conf}}$ , which is applied to remove inaccurate detections on original images. As a result, SMR for the object detection task represents the proportion of machines with higher mAPs than a reasonable threshold.

The ground truth class labels annotated by humans are excluded in the SMR calculation process for three reasons. First, humans may make mistakes during the annotation, resulting in problematic SMR modeling. Second, the difference in analysis results on original images and their distorted variants inherently reveals the MVS characteristics in terms of compression. Third, without the need for annotations, we can study the SMR profiles with an unlimited number of images and videos in an unsupervised manner. Such annotation method has been proven to be reasonable in [21], [56], [96].

The satisfaction score functions in Eq. (5) (6) can be used to find the JND points for machine  $M_j$  to image  $I_0$ . For the image classification task, JND points locate at QPs where

$$S(M_j; I_{q_i}) = 0. \quad (7)$$

For the object detection task, JND points locate at QPs where

$$S(M_j; I_{q_i}) < T_S. \quad (8)$$

On these QPs, machine perceptions deviate noticeably from the original image and become unreliable or even unusable. Hence, the satisfaction score directly reflects a machine's JND characteristics. SMR further mitigates the biases from a few specific machines and measures the compression quality accurately with the general MVS characteristics captured. Images with larger SMRs are more friendly to machine vision applications because it is more likely to get correct analysis results on such images for any machine. The significance of SMR further increases when the machine used for analysis is unknown before compression, or in a long term that the machine can be upgraded or replaced,

which are common in the real world. More importantly, SMR can guide the compression to remove perceptual redundancy for MVS and maintain the same machine perceptions on original and compressed images for most machines, achieving an optimal balance among compression efficiency, generalizability, and machine analysis performance. Therefore, SMR is a more reasonable optimization target for VCM and fuels the perceptual coding for MVS.

## 5 SMR DATASET

In this section, we build the first SMR dataset to facilitate SMR studies. There are three steps: image preparation, machine library construction, and SMR annotation.

### 5.1 Image preparation

A large number of high-quality images with different semantic information are required to build a good SMR dataset. As the images are used to calculate satisfaction scores according to the difference in machine analysis results, it is reasonable to utilize existing commonly-used machine vision task datasets that have been properly constructed. In this work, we choose MS COCO 2017 as the source dataset. Similar to section 3, all COCO images are compressed as intra video frames using HM-16.24. We select 36 QPs at this time, which are 11, 13, 15, 17, 19, 21, 22, . . . , and 51. It should be mentioned that HEVC is not only a video coding standard, but can also be applied for image compression with the intra mode. Moreover, HEVC is more advanced and efficient than most still image compression standards like JPEG, thus we can find more generalized and applicable SMR profiles for both images and videos.

### 5.2 Machine library construction

As described in section 3, the diversity of machines exists universally, even when they have relatively small differences in structure or scale. As a result, to obtain a more accurate SMR, we should include as many different machines as possible for the satisfaction score calculation and aggregation. However, it is impractical to consider every machine in the infinite set  $\mathbb{M}$ . Therefore, we need to sample a proportion of all machines to form a subset  $\mathcal{M}$  such that

$$\text{SMR}_{\mathcal{M}}(I_{q_i}) \simeq \text{SMR}_{\mathbb{M}}(I_{q_i}), \quad \mathcal{M} \subset \mathbb{M}. \quad (9)$$

There are several factors to consider for building a representative and useful  $\mathcal{M}$ , including machine's capability, architecture, size, complexity, and the number of machines. The machine's capability is the most important attribute that directly determines the analysis task accuracy. However, we should not just include machines with state-of-the-art performance in the library because many other less capable machines have their own advantages and application scenarios. For instance, some machines have simpler structures and are easier to implement and accelerate with hardware. Some machines have much fewer parameters, which are more appropriate in stringent memory and computation complexity environments. Some other machines can run fast in low latency, satisfying real-time processing requirements.

TABLE 2

SMR machine library for image classification. References to these machines are omitted for better presentation, which can be found at [97].

Version	Category	Name
v1	Classical CNN	AlexNet
		VGG-11, VGG-13, VGG-16, VGG-19, VGG-11-bn, VGG-13-bn, VGG-16-bn, VGG-19-bn
		GoogLeNet; Inception-v3
		ResNet-18, ResNet-34, ResNet-50, ResNet-101, ResNet-152
		ResNeXt-50-32x4d, ResNeXt-101-32x8d; Wide-ResNet-50, Wide-ResNet-101
		DenseNet-121, DenseNet-161, DenseNet-169, DenseNet-201
	Lightweight Network	ShuffleNet-v2-x0.5, ShuffleNet-v2-x1.0
		MobileNet-v2, MobileNet-v3-Small, MobileNet-v3-Large
	Network Architecture Search	MNASNet-0.5, MNASNet-1.0
		EfficientNet-B0, EfficientNet-B1, EfficientNet-B3, EfficientNet-B5, EfficientNet-B7 RegNet-x-400MF, RegNet-x-800MF, RegNet-x-1.6GF, RegNet-x-3.2GF, RegNet-x-8GF, RegNet-x-16GF, RegNet-x-32GF; RegNet-y-400MF, RegNet-y-800MF, RegNet-y-1.6GF, RegNet-y-3.2GF, RegNet-y-8GF, RegNet-y-16GF, RegNet-y-32GF
Transformer	ViT-b-16, ViT-b-32, ViT-l-16, ViT-l-32	
Modern CNN	ConvNeXt-Tiny, ConvNeXt-Small, ConvNeXt-Base, ConvNeXt-Large	
v2	Classical CNN	ResNeXt-101-64x4d
	Lightweight Network	ShuffleNet-v2-x1.5, ShuffleNet-v2-x2.0
	Network Architecture Search	MNASNet-0.75, MNASNet-1.3; EfficientNet-B2, EfficientNet-B4, EfficientNet-B6; EfficientNet-v2-S, EfficientNet-v2-M, EfficientNet-v2-L
	Transformer	Swin-T, Swin-S, Swin-B

TABLE 3

SMR machine library for object detection. References to these machines are omitted for better presentation, which can be found at [98].

Method	Backbones/Variants
Faster R-CNN	ResNet-50, ResNet-101, ResNeXt-101-32x4d, ResNeXt-101-32x8d, ResNeXt-101-64x4d
	ResNet-50-DCN, ResNet-101-DCN, ResNeXt-101-32x4d-DCN
	Res2Net-101; ResNeSt-50, ResNeSt-101
	RegNet-x-400MF/800MF/1.6GF/3.2GF/4GF
RetinaNet	ResNet-50, ResNet-101, ResNeXt-101-32x4d, ResNeXt-101-64x4d
	ResNet-50-NAS-FPN
	PVTv2-B0/B1/B2/B3/B4/B5 RegNet-x-800MF/1.6GF/3.2GF
Cascade R-CNN	ResNet-50, ResNet-101, ResNeXt-101-32x4d, ResNeXt-101-64x4d
	ResNet-50-DCN, ResNet-101-DCN
	Res2Net-101; ResNeSt-50, ResNeSt-101
SSD	SSD VGG-16-512; SSD-Lite MobileNet-v2
FCOS	ResNet-50, ResNet-101, ResNeXt-101-64x4d
FoveaBox	ResNet-50, ResNet-101
RepPoints	ResNet-50, ResNet-101, ResNeXt-101-32x4d-DCN
Grid R-CNN	ResNet-50, ResNet-101, ResNeXt-101-32x4d, ResNeXt-101-64x4d
FSAF	ResNet-50, ResNet-101, ResNeXt-101-64x4d
Generalized Focal Loss	ResNet-50, ResNet-101, ResNet-101-DCNv2, ResNeXt-101-32x4d, ResNeXt-101-32x4d-DCNv2
PAA	ResNet-50, ResNet-101
DETR	DETR ResNet-50; Deformable DETR ResNet-50; Deformable DETR ResNet-50 (refined)
YOLOX	YOLOX-tiny/s/l/x
YOLOv5	YOLOv5-n/s/m/l-640, YOLOv5-n/s/m/l-1280
PP-YOLOE+	PP-YOLOE+-s/m/l/x
YOLOv7	YOLOv7-tiny/l/x-640, YOLOv7-w/e-1280
YOLOv8	YOLOv8-n/s/m/l/x
Others	Dynamic R-CNN ResNet-50
	DetectoRS Cascade R-CNN ResNet-50
	CornerNet HourglassNet-104
	CentripetalNet HourglassNet-104
	AutoAssign ResNet-50 DyHead ATSS ResNet-50

Moreover, many machines have already been widely used due to historical reasons and are costly to replace. Last but not least, the number of machines should be sufficient to remove the bias from just a few machines. In summary, as proved in section 3, the diversity of machines needs to be carefully considered during the machine library construction to capture the general MVS characteristics more thoroughly and accurately.

In this work, we conscientiously review the growth and current state of the machine vision community and select several representative machines to construct machine libraries. For the image classification task, we build two versions. The information of selected machines is presented in TABLE 2, where the leftmost column shows the library version. Note that v2 is built upon v1 so that it contains all machines from v1. The middle column shows the category of these machines, and the rightmost column shows their names. In total, the machine libraries v1 and v2 consist of 58 and 72 machines, respectively. Their top-1 prediction accuracies on ImageNet range from 60% to 88%, sizes range from 1.4 to 300 millions of parameters, and complexities range from 0.1 to 360 GFLOPs. Both cutting-edge transformers and aged CNNs, complicated and lightweight machines, and hand-crafted and automatically-searched machines are included. We also consider machines in the same architecture but have different depths or scales. All machines' initial weights are from PyTorch [95], [97], and we fine-tune them on the original COCO train2017 dataset using cropped object images to adapt to COCO semantics.

For the object detection task, we build a machine library with 98 machines to embrace the rapid development in this area. The information of selected machines is presented in TABLE 3, where the first column shows the machines' names and the second column presents the neural network backbones that they use to extract features or their variants in different sizes. These machines' mAPs on COCO val2017 dataset range from 21.3 to 55.1, sizes range from 1.8 to 200 millions of parameters, and inference speed ranges from less than one frame-per-second (fps) to 1000 fps. Both CNN-based and transformer-based, one-stage and two-stage, performance-targeted and speed-targeted machines are included in this library. Moreover, we take the cases where the detector keeps the same but uses different backbone networks into account. All machines' weights are from MMDetection [98], [99], which are trained on the original COCO train2017 dataset.

Despite the fullness of diversity, the number of machine subjects in the constructed libraries are notably larger compared to most HVS-oriented JND and SUR datasets such as VideoSet [52] (around 30 human subjects per video) or [100] (42 subjects per image). We believe that it is sufficient to study and model SMR with this library from a practical perspective. Additionally, including fewer machines will bring some negative impacts, which will be described later in section 5.4.

### 5.3 SMR annotation

Due to the lack of bounding box annotations on the COCO test dataset, we randomly select 10000 original images from the COCO train2017 dataset to form our SMR test dataset

and keep the validation set the same. After compression, each original COCO image or object image will have 36 distorted variants. We use Eq. (4) to (6) to generate ground truth SMR labels for all of them, including the originals. For the image classification task, SMR labels are annotated for object images that have more pixels than  $32 \times 32$ . We set  $K = 1, 3, 5$  in Eq. (5) and use two versions of machine libraries for the annotation separately, resulting in six types of SMR, namely SMR-top1-v1/v2, SMR-top3-v1/v2, and SMR-top5-v1/v2, respectively. For the object detection task, SMR labels are annotated for all images. We set  $T_{\text{IOU}}$  to  $[0.5 : 0.95 : 0.05]$  (which means values range from 0.5 to 0.95 with a step of 0.05) and  $T_{\text{conf}}$  to 0.3 in Eq. (6), and set  $T_S$  to  $[0.5 : 0.95 : 0.05]$  in Eq. (4). Hence, there are  $10 \times 10 = 100$  types of SMR for object detection. Eventually, for the image classification task, the constructed SMR dataset contains  $617479 \times (36 + 1) = 22846723$  images and more than 137 million SMR labels. There are 20052335, 936396, and 1857992 images for train, validation, and test dataset, respectively. For the object detection task, the constructed SMR dataset contains  $123287 \times (36 + 1) = 4561619$  images and more than 456 million SMR labels. There are 4006619, 185000, and 370000 images for train, validation, and test dataset, respectively. The scale of our SMR dataset is marvelous. We believe that it can establish a solid foundation for not only this work but also SMR studies in the future.

### 5.4 Dataset study

We plot several QP-SMR curves of randomly selected images in Fig. 1 to give a first impression of how SMR curves look. It can be obviously observed that different images have different QP-SMR curves, thus the image's SMR is a content-related attribute. The distributions of SMR of the SMR dataset, *i.e.* average SMR values under different QPs, are also presented in Fig. 2. Both the QP-SMR curve of a specific image and the QP-SMR distributions of the SMR dataset can again prove the diversity of machines because if all machines have identical MVS characteristics, SMR should either always be 0 (no machine is satisfied with the compression quality) or 1 (every machine is satisfied with the compression quality), which is opposite against the truth.

Generally, SMR tends to decrease as QP increases, but the amplitude changes between QPs. When QP is small, SMR is decreased just slightly in most cases. While at large QPs, SMR often drops noticeably and becomes unusable under heavy compression. Interestingly, there can be significant SMR variations even between neighboring QPs for a certain image, indicating that QP and SMR do not have a monotonic correlation. In other words, a larger QP may lead to a higher SMR, or a worse compression quality may lead to more similar machine perceptions with original images. This finding is very important for three reasons. First, **many machines behave unstably in a similar way when facing compression distortions**. It is expected that a specific machine may have its own flaw that cannot distinguish good and bad compression quality precisely. But when many machines are considered all together, this uncertainty is anticipated to be erased, which is unfortunately not true. Second, it reveals that **the JND characteristics of MVS are inconsistent in**



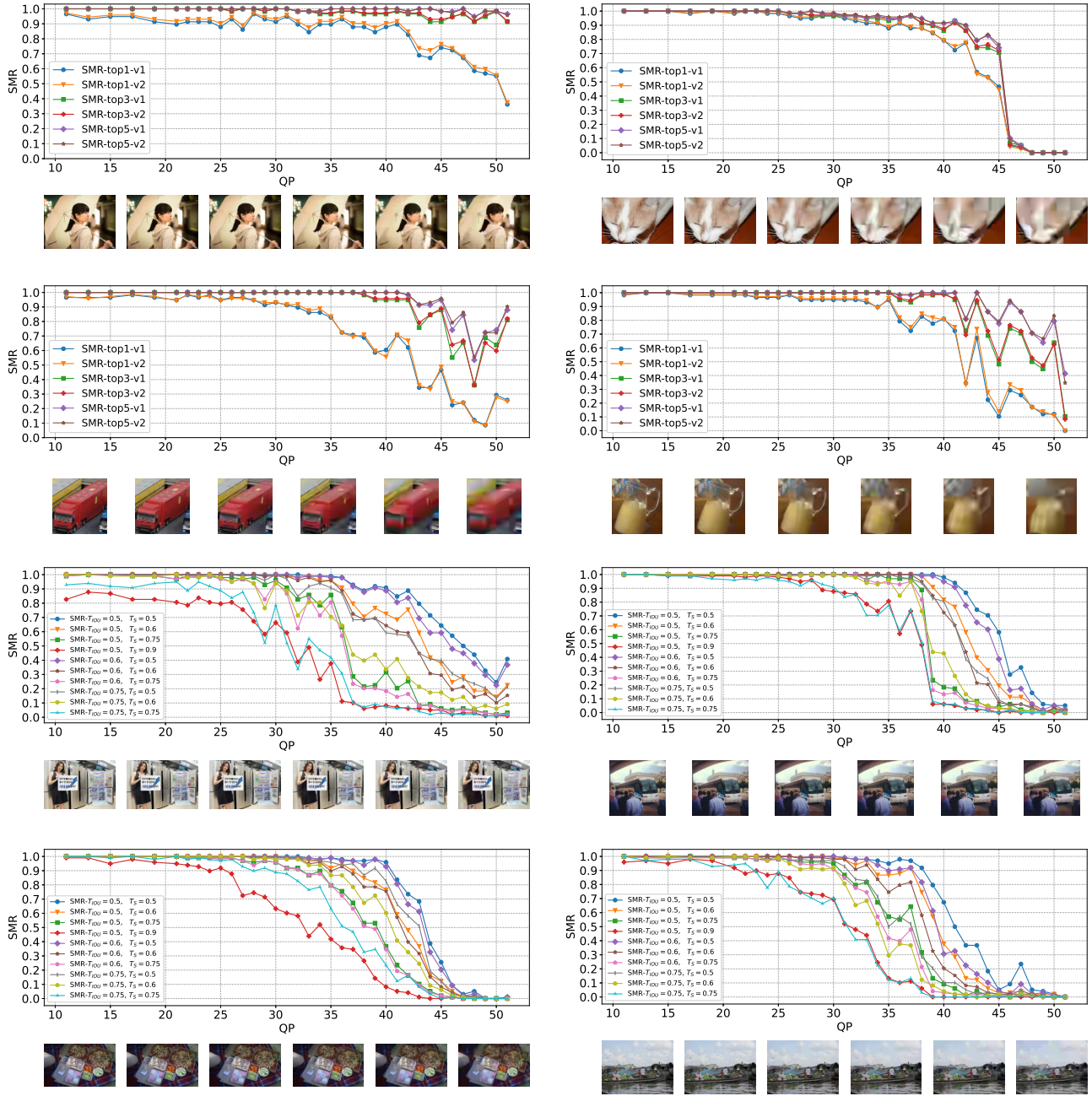


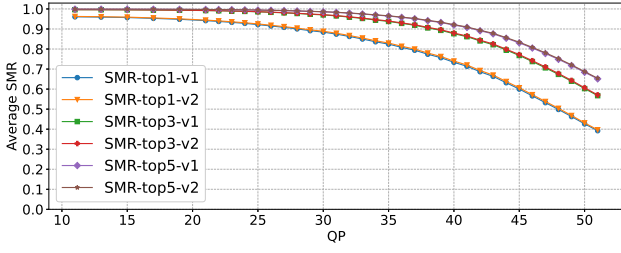
Fig. 1. QP-SMR curves of several randomly selected images. The corresponding object image and its compressed versions are displayed under the curve, where the leftmost one is the original object image, and the rest are compressed variants with QP = 32, 40, 45, 48, and 51, respectively. Top 4 sub-figures are for the image classification task, and the bottom 4 figures are for the object detection task.

**the context of image and video coding.** Take the image classification task as an example. As described in section 4, the first machine JND point should locate at the minimum QP denoted by  $q_{\min}$  that  $S(M_j; I_{q_{\min}}) = 0$ . However, it cannot be assured that  $\forall q_x > q_{\min}, S(M_j; I_{q_x}) \equiv 0$ . For the object detection task, the situation is similar. Third, it demonstrates that it is possible to obtain a higher SMR under heavier compression, which is ideal for VCM because both lower bit-rate and better analysis performance for many machines can be achieved at the same time.

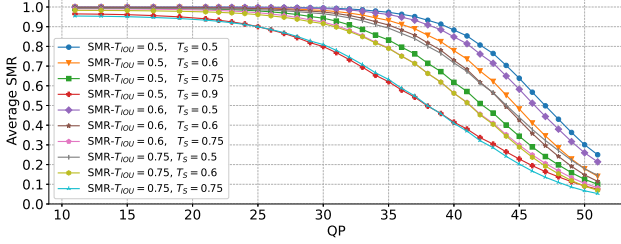
Moreover, the characteristics and distributions of different types of SMR are distinctive. For the image classification

task, at the same QP,  $SMR\text{-top5} \geq SMR\text{-top3} \geq SMR\text{-top1}$ . For the object detection task, SMR is jointly controlled by  $T_{IOU}$  and  $T_S$ , but typically  $T_S$  has a greater weight. It is hard or even impossible to estimate an unknown type of SMR with a known type of SMR. Moreover, the trend of SMR variation also differs for different types of SMR. For example,  $SMR\text{-top5}(I_{q_i}) > SMR\text{-top5}(I_{q_j})$  doesn't always lead to  $SMR\text{-top1}(I_{q_i}) > SMR\text{-top1}(I_{q_j})$ .

Regarding v1 and v2 machine libraries for the image classification task, their SMR values are closed. Numerically, in the SMR dataset, without counting original images, the mean absolute errors (MAE) of SMR-top1/3/5 between v1



(a) Image classification



(b) Object detection

Fig. 2. QP-SMR distributions of the SMR dataset for different machine analysis tasks.

TABLE 4

Differences of SMRs that are obtained from different number ( $N_m$ ) of machine subjects and from v1/v2 machine library, which are measured by MAE. \* indicates that the machines are manually selected, otherwise, they are randomly selected from the v2 machine library.

$N_m$	10	12*	20	30	40	50	60	70
58 (v1)	0.051	0.047	0.034	0.028	0.022	0.016	0.013	0.012
72 (v2)	0.051	0.044	0.033	0.025	0.019	0.013	0.009	0.004

and v2 libraries are 0.011, 0.007, and 0.005, and the standard deviations are 0.024, 0.016, and 0.014, respectively. We further compare the SMR from different number of machine subjects. In this comparison, machines are randomly picked from the v2 library, and SMRs-top1 values are re-calculated denoted by  $SMR_{N_m}$ , where  $N_m$  is the number of machines. We also investigate a special case where machines are the 12 ones used in section 3, which were proven to be full of diversity. MAEs of  $SMR_{N_m}$  values are computed among 10,000 groups of compressed images that are also randomly selected, each in all 36 quality levels. For each  $N_m$ , the comparison will be performed three times to obtain averaged MAE results, which are presented in TABLE 4. According to the results, as  $N_m$  increases,  $MAE(SMR_{N_m}, SMR_{58/72})$  decreases, although there are still small differences at last. It is expected that as the number of machines in  $\mathcal{M}$  increases,  $SMR_{\mathcal{M}}(I_{q_i})$  converges to  $SMR_{\mathbb{M}}(I_{q_i})$ . On the other hand, a smaller  $N_m$  inevitably leads to less accurate general MVS characteristics capturing due to the diversity of machines, which again demonstrates that we cannot just consider one or only very few of them in VCM.

## 6 SMR MODELING

SMR can serve as an assessment metric for VCM to evaluate the machine perception consistency for the majority of machines under different compression quality levels. Then the evaluation result can be used for improving the

VCM encoder to remove perceptual redundancy for MVS by finding the most appropriate coding parameters, or being the target during rate-distortion optimization process, etc., achieving higher SMR values under the similar bit-rate. However, in the real world, it is too time- and resource-consuming to collect satisfaction scores from every machine in the machine library and aggregate them into a final accurate SMR. Therefore, it is essential to predict the SMR of an image or video frame with a simpler model.

Ideally, we would like to have an omnipotent model that can directly predict the entire SMR curve for an original image across all possible compression quality levels, enabling the VCM encoder to determine the optimal operation point easily. However, it seems impossible to build such a model due to the lack of prior knowledge about how quality changes with compression rate, particularly when there can be significant SMR variations between similar quality levels. Therefore, we propose the task of SMR prediction or SMR modeling for VCM in the following formulation: with image or video frame  $I_{q_i}$  in compression quality level  $q_i$  being the distorted variant of the original image or video frame  $I_0$ , the goal is to design a model  $G_\theta$  such that

$$G_\theta(\mathcal{I}) = SMR(I_{q_i}), \quad (10)$$

where  $\theta$  is a set of learnable parameters of the model, and  $\mathcal{I}$  is a set of input images that either  $\mathcal{I} = \{I_{q_i}, I_0\}$  or  $\mathcal{I} = \{I_{q_i}\}$ , resulting in two kinds of SMR modeling tasks, which are full-reference and no-reference SMR modeling, where the reference is the original image  $I_0$ .

In this work, we make an initial attempt to study the full-reference SMR modeling task. Since SMR is a continuous decimal value in the range of  $[0, 1]$ , SMR modeling can be regarded as a regression task. According to section 5.4, the SMR profile is content-related, so we propose a data-driven method based on deep learning to predict SMR independently for any image or video frame. Specifically, we design a neural network consisting of two parts: an encoder  $E(\cdot)$  and a regressor  $R(\cdot)$ . The encoder  $E(\cdot)$  encodes the input image  $x \in \mathbb{R}^{3 \times H \times W}$  into a latent representation  $h \in \mathbb{R}^d$ , where  $H$  and  $W$  are height and width of the image and  $d$  is the number of dimensions of  $h$ . The regressor  $R(\cdot)$  receives the generated representations from both original and compressed images as inputs, and finally outputs an estimated SMR of the compressed image.

Here, the key is to learn a distinguishable and robust representation that can be used to predict the similarity of machine perceptions under different compression quality levels. Since machines perceive, understand, and analyze images by extracting high-level semantic features, it is reasonable to assume that deep features can inherently be good representations for this task and have a strong correlation with SMR values. To verify the assumption, we first extract deep features from image  $I_0$  and all of its compressed versions using every machine in the v1 machine library, which are denoted as  $f_{M_j}^0$  or  $f_{M_j}^{q_i}$ . Then, for each compression quality level, a features difference value is calculated by

$$D(f_{M_j}^{q_i}) = \cos(f_{M_j}^{q_i}, f_{M_j}^0), \quad (11)$$

which will be averaged across all machines. After that, the correlation between mean features difference and SMR

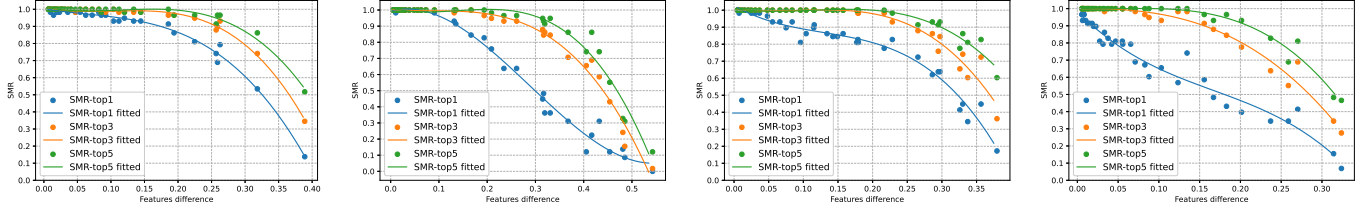


Fig. 3. The non-linear negative correlations between mean features difference and SMR for several images in the SMR dataset.

can be investigated. Several samples are shown in Fig. 3, where the curves are fitted cubically as a reference. It can be observed that there is a consistent non-linear negative correlation between these two variables. Therefore, the extracted deep features are appropriate representations for SMR modeling.

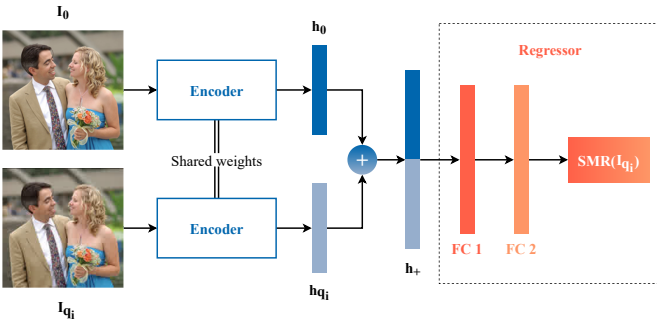


Fig. 4. The proposed full-reference SMR prediction model.

Based on the investigation, we propose a simple but effective model  $G$  as a baseline for the SMR prediction task, which is illustrated in Fig. 4. The encoder  $E(\cdot)$  is a Siamese neural network trained for machine analysis tasks like image classification but with fully-connected (FC) layers removed. It extracts features from  $I_0$  and  $I_{q_i}$  to produce the corresponding image representations  $h_0$  and  $h_{q_i}$ . Then, we concat  $h_0$  and  $h_{q_i}$  to form an embedding  $h_+ \in \mathbb{R}^{2d}$  that implicitly contains the features difference information. Finally,  $h_+$  is sent to the regressor  $R(\cdot)$  to predict  $\text{SMR}(I_{q_i})$ , which is a multi-layer perceptron (MLP) that can learn the non-linear correlation between features difference and SMR. The training objective is to minimize the L1 distance:

$$\min |R(E(I_0) \oplus E(I_{q_i})), \text{SMR}(I_{q_i})|. \quad (12)$$

One major drawback of the baseline SMR prediction model  $G$  is that it does not take full advantage of all labeled data. More specifically, it only leverages the information from the SMR difference between the original image and its compression version. However, we can actually further utilize the SMR difference between the two compression variants to generate better image representations for capturing the SMR characteristics. Hence, we design another model  $Q_\phi$  such that

$$Q_\phi(I_{q_i}, I_{q_j}) = |\text{SMR}(I_{q_i}) - \text{SMR}(I_{q_j})|, \quad (13)$$

where  $\phi$  is a set of learnable parameters. The structure as well as the training objective of  $Q_\phi$  remain the same as the

baseline model, as this auxiliary task is also a regression task accomplished by extracting good embeddings. After the training is finished, this SMR difference-based model  $Q$  can predict the SMR of  $I_{q_i}$  by:

$$\hat{\text{SMR}}(I_{q_i}) = 1.0 - Q(I_0, I_{q_i}). \quad (14)$$

## 7 EXPERIMENTS

In this section, we conduct extensive experiments to prove the effectiveness and generalizability of proposed SMR models. We will use *cls* and *det* as abbreviations for the image classification and object detection task, respectively.

### 7.1 Implementation details

We use an EfficientNet-B4 pre-trained on ImageNet as  $E(\cdot)$  to encode the original and compressed image into representations with  $d = 1792$  for both baseline model  $G$  and SMR difference-based model  $Q$ . The input and output dimensions of FC layers in  $R(\cdot)$  are  $(1792 \times 2, 4096)$ ,  $(4096, 4096)$ , and  $(4096, 1)$ , respectively, with a ReLU module placed between neighboring FC layers. The baseline SMR models are trained on three NVIDIA RTX4090 GPUs, and the SMR difference-based models are trained on seven NVIDIA RTX3090 GPUs to speed up convergence. We use automatic mixed precision technique to accelerate training. The input image resolutions are aligned with machines for different analysis tasks, and the batch sizes also change along with the resolutions to fill GPU memory. Specifically, for *cls*, input object images are resized to  $224 \times 224$ , and the batch size is set to  $N_{\text{GPU}} \times 92$ , where  $N_{\text{GPU}}$  is the number of GPUs. For *det*, input images are resized to  $512 \times 512$ , and the batch size is set to  $N_{\text{GPU}} \times 18$ . We train the SMR models using the Adam optimizer with a learning rate of  $10^{-4}$ . To avoid any potential effects on an image's SMR, no data augmentation is used. For the baseline models, we train them on the SMR training dataset for 10 iterations. For the SMR difference-based models, since the two compression quality levels  $q_i$  and  $q_j$  are randomly picked for each data sample during the training process, we train them for 1000 iterations to leverage more training labels.

### 7.2 Evaluation methods and metrics

The SMR prediction error rate is straight given by the L1 loss during training and testing, but we also want to evaluate the coding performance improvement using the SMR model. In the real world, applications would expect compressed images and videos to have higher SMRs than a customizable threshold  $T_{\text{SMR}}$ . To achieve the target, the simplest way

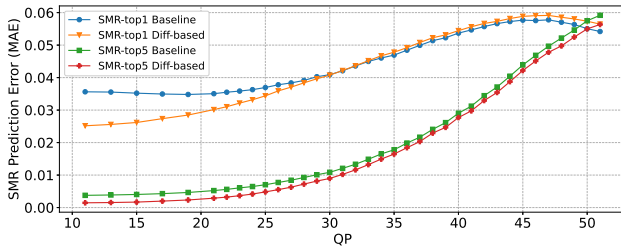


is to select a constant QP for the compression according to a known QP-and-average-SMR distribution. However, compressing with constant QPs cannot reach optimal results for every image because many of them can be compressed with larger QPs without violating the SMR target, which has been explained in section 5.4. Therefore, we use predicted SMRs to increase compression efficiency for VCM in the following steps:

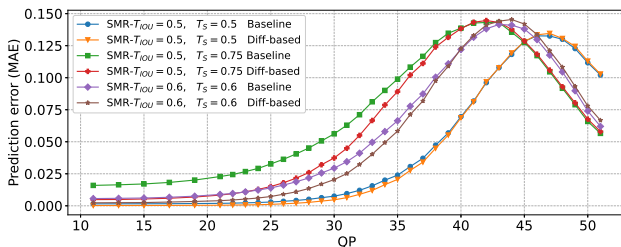
- 1) We choose a series of SMR thresholds to form a set  $\mathbb{T}_{SMR}$ . For each threshold  $T_{SMR}$  in  $\mathbb{T}_{SMR}$ , referring to a known QP-and-average-SMR distribution  $\mathcal{D}_{SMR} = \{\overline{SMR}_{q_1}, \overline{SMR}_{q_2}, \dots, \overline{SMR}_{q_n}\}$ , we can select a QP  $q_b$  satisfying  $\overline{SMR}_{q_b} \geq T_{SMR}$  as the baseline. If there isn't any QP value that can satisfy such condition, we select the one that has the minimum  $|\overline{SMR}_{q_b} - T_{SMR}|$ .
- 2) We predict the SMRs of images compressed with QP =  $q_b, q_{b+1}, q_{b+2}, \dots, q_n$  using the proposed SMR model. The predicted SMRs are denoted as  $SMR_{pred}(\cdot)$ .
- 3) We search the predicted SMRs reversely to find the first one satisfying  $SMR_{pred}(I_{q_{b+k}}) \geq T_{SMR}$ , and consider  $q_{b+k}$  to be the best QP to compress  $I_0$ .

After that, the average bit-rates in bits per pixel (bpp) as well as the mean **actual** SMRs under all SMR thresholds are recorded, which forms multiple rate-SMR curves. The coding performance is then evaluated by Bjøntegaard Delta rate (BD-rate) [101], which corresponds to the average bit-rate difference **in percent** for the same SMR, the lower the better. Note that some original images may have lower SMRs than  $T_{SMR}$  for all QPs in the search interval. In such case,  $q_b$  is used for the compression.

### 7.3 Basic results



(a) Image classification



(b) Object detection

Fig. 5. The distribution of SMR prediction errors under different QPs.

As a demonstration, we select several types of SMR to train the proposed SMR models. More specifically, for *cls*, we train two pairs of baseline and SMR difference-based models (4 models in total) to predict SMR-top1 and SMR-top5 using the SMR labels annotated by the v1 machine

library. For *det*, we train three pairs of baseline and SMR difference-based models to predict SMR with  $(T_{IOU}, T_S)$  set to  $(0.5, 0.5)$ ,  $(0.5, 0.75)$ , and  $(0.6, 0.6)$  (6 models in total). Predicting other types of SMR should be similar. The MAE between all predicted and actual SMRs of the two targeted tasks can be checked in TABLE 5 (3rd column) and 6 (4th column), respectively, and the distributions of MAEs under different QPs are presented in Fig. 5. It can be observed that for *cls*, QP and SMR prediction error have an overall positive correlation, implying that larger QPs result in higher SMR prediction errors. For *det*, such correlation becomes more non-monotonic: the lowest prediction performance is reached in the QP range of  $[42, 47]$ . The reason is that SMRs for *det* are consistently low at large QPs, making prediction easier when the models find there are huge differences between extracted representations from original and compression versions of images. When the QP is large but not large enough, however, the features difference becomes more ambiguous, leading to inaccurate SMR predictions.

We then use the method described in section 7.2 to evaluate the coding efficiency optimized with SMR. For SMR-top5 of *cls*,  $\mathbb{T}_{SMR} = [0.75 : 0.05 : 0.95]$ , which means values range from 0.75 to 0.95 with a step size of 0.05. For other types of SMR of *cls* and *det*,  $\mathbb{T}_{SMR} = [0.6 : 0.05 : 0.95]$ . The resulting rate-SMR curves are shown in Fig. 6, where "HEVC" is the compression results by constant QPs, "GT" is the optimized results by applying ground truth SMRs, "Pred Baseline" is by applying predicted SMRs from baseline models, and "Pred Diff-based" is by applying predicted SMRs from SMR difference-based models. More precise and numerical results are presented in TABLE 5 (3rd column) and 6 (4th column).

Several conclusions can be drawn from these results: (1) Using ground truth SMRs to determine appropriate QPs dramatically improves coding performance for machines. For *cls*, the BD-rate savings are 38.2% and 43.0% for SMR-top1 and SMR-top5, respectively. For *det*, the BD-rate savings are 19.1%, 21.9%, and 20.8% for the three  $(T_{IOU}, T_S)$  pairs, respectively. As a reference, the state-of-the-art coding standard VVC exceeds the last-generation standard HEVC by around 30% [104]. (2) Using predicted SMRs also increases coding efficiency considerably, though not achieving the best performance due to prediction errors, demonstrating the effectiveness of the proposed SMR models. (3) SMR difference-based models consistently outperform baseline models by achieving lower prediction error and higher BD-rate saving, showing its superiority in the full-reference SMR modeling task. (4) The optimal/practical coding gains achieved with ground truth/predicted SMR differ by tasks. The coding gains are more remarkable for *cls* than *det*. The main reason is that *cls* is an easier task than *det* that more images can preserve a high SMR after heavy compression as illustrated in Fig. 2. Hence, it is more possible to select larger QPs during the optimization, saving more bits while still satisfying enough number of machines. (5) Coding gains are also influenced by different types of SMR. For *cls*, the prediction of SMR-top5 is notably more accurate than SMR-top1 under almost every QP, and thereby the coding efficiency increment is more significant. For *det*, the maximum coding gain is achieved when  $(T_{IOU}, T_S) = (0.5, 0.75)$ , though its prediction appears to be the most inaccurate one

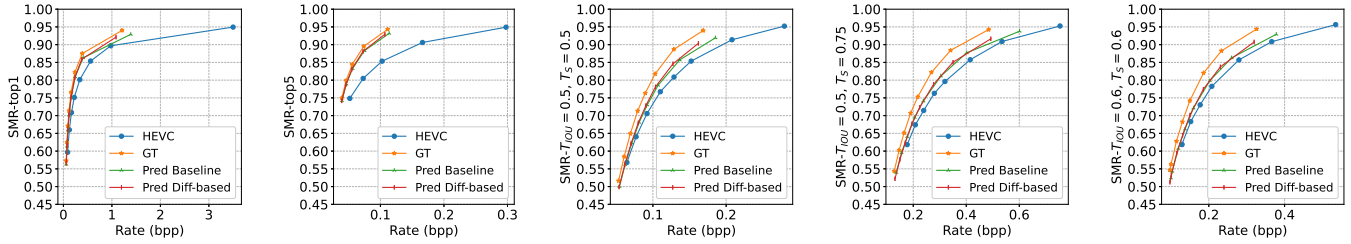


Fig. 6. Rate-SMR curves for all types of SMR of the two targeted tasks using ground truth SMR, predicted SMR from baseline models, and predicted SMR from SMR difference-based models to optimize QP selection, respectively.

TABLE 5

The SMR prediction performance and coding efficiency improvements of SMR models for the image classification task on different machine library versions, codecs, and datasets.

Dataset-Codec		COCO-HEVC		COCO-VVC		COCO-AVS3		COCO- [102]		COCO- [103]		VOC-HEVC		TVDI-VVC	
Machine library version		v1	v2	v1	v2	v1	v2	v1	v2	v1	v2	v1	v2	v1	v2
SMR-top1	MAE Baseline	0.0463	0.0454	0.0474	0.0533	0.0494	0.0549	0.1005	0.1054	0.1050	0.1091	0.0370	0.0468	0.0567	0.0610
	MAE Diff-based	0.0434	0.0417	0.0451	0.0554	0.0481	0.0569	0.1061	0.1113	0.1113	0.1157	0.0450	0.0593	0.0663	0.0780
	BD-rate GT	<b>-38.2</b>	<b>-38.1</b>	<b>-37.0</b>	<b>-37.7</b>	<b>-40.7</b>	<b>-41.7</b>	<b>-11.4</b>	<b>-10.1</b>	<b>-12.2</b>	<b>-10.9</b>	<b>-38.7</b>	<b>-39.2</b>	<b>-42.2</b>	<b>-42.7</b>
	BD-rate Pred Baseline	-28.6	-30.7	-25.6	-26.5	-30.9	-32.0	-5.3	-5.1	-5.6	-5.4	-30.8	-30.7	-34.2	-34.8
	BD-rate Pred Diff-based	-29.8	-31.9	-26.8	-27.8	-32.1	-33.3	-6.1	-6.0	-6.3	-6.2	-33.1	-33.9	-36.4	-37.9
SMR-top5	MAE Baseline	0.0217	0.0211	0.0219	0.0385	0.0251	0.0404	0.0349	0.0368	0.0343	0.0359	0.0154	0.0355	0.0245	0.0395
	MAE Diff-based	0.0197	0.0189	0.0206	0.0405	0.0236	0.0421	0.0364	0.0384	0.0352	0.0370	0.0150	0.0367	0.0242	0.0433
	BD-rate GT	<b>-43.0</b>	<b>-42.9</b>	<b>-42.2</b>	<b>-45.9</b>	<b>-43.2</b>	<b>-48.4</b>	<b>-16.8</b>	<b>-14.4</b>	<b>-19.8</b>	<b>-18.2</b>	<b>-32.7</b>	<b>-41.7</b>	<b>-43.8</b>	<b>-49.2</b>
	BD-rate Pred Baseline	-37.4	-38.0	-36.4	-39.2	-37.3	-41.6	-7.9	-6.7	-9.0	-8.8	-28.8	-36.3	-37.4	-41.5
	BD-rate Pred Diff-based	-38.1	-38.7	-36.9	-39.6	-37.8	-42.1	-9.5	-8.2	-10.8	-10.5	-29.1	-36.5	-37.9	-41.7

TABLE 6

The SMR prediction performance and coding efficiency improvements of SMR models for the object detection task on different machine library versions and codecs.

$T_{IOU}$	$T_S$	Codec	HEVC	VVC	AVS3	[102]	[103]
0.5	0.5	MAE Baseline	0.0442	0.0451	0.0566	0.0159	0.0149
		MAE Diff-based	0.0429	0.0486	0.0583	0.0174	0.0155
		BD-rate GT	<b>-19.1</b>	<b>-20.2</b>	<b>-21.8</b>	-	-
		BD-rate Pred Baseline	-7.8	-5.3	-7.8	-	-
		BD-rate Pred Diff-based	-9.2	-4.5	-8.6	-	-
0.5	0.75	MAE Baseline	0.0730	0.0733	0.0872	0.0629	0.0586
		MAE Diff-based	0.0644	0.0763	0.0901	0.0775	0.0683
		BD-rate GT	<b>-21.9</b>	<b>-21.9</b>	<b>-22.7</b>	<b>-14.8</b>	<b>-17.4</b>
		BD-rate Pred Baseline	-9.2	-7.2	-7.6	-1.4	-1.2
		BD-rate Pred Diff-based	-9.8	-4.7	-6.7	-1.5	-2.4
0.6	0.6	MAE Baseline	0.0599	0.0632	0.0779	0.0402	0.0374
		MAE Diff-based	0.0569	0.0699	0.0824	0.0473	0.0417
		BD-rate GT	<b>-20.8</b>	<b>-20.4</b>	<b>-21.5</b>	<b>-17.6</b>	<b>-19.6</b>
		BD-rate Pred Baseline	-7.7	-4.2	-5.2	-1.4	-3.3
		BD-rate Pred Diff-based	-8.3	-1.9	-4.5	-1.9	-3.1

considering all QPs. For other two types of SMR, the coding gains are similar. The main reason is that the predictions of SMR with  $(T_{IOU}, T_S) = (0.5, 0.75)$  are actually more accurate under larger QPs ( $QP \geq 45$ ). In such cases, correct predictions can bring much more bit-rate savings than ones under lower QPs.

#### 7.4 Generalize to more machines

As a demonstration to verify the generalizability of our SMR models on more machines, we assess the SMR models for *cls* on the v2 machine library. Since these models are trained on v1 machine library, the additional 14 machines are unknown to them. Experimental results are shown in TABLE 5 (4th

column). It is interesting to find that the prediction errors are even decreased, and slightly more coding gains can be achieved. Moreover, the difference of prediction error rate between v1 and v2 machine library is smaller than that of the ground truth SMRs of the two versions. Consequently, the proposed SMR models learn robust and generalizable representations that capture the perceptual characteristics of general machines.

#### 7.5 Generalize to unseen codecs

In the real world, applications may use different codecs, an ideal SMR model should generalize well to all of them. To verify such generalizability, we evaluate the proposed SMR models on various codecs, including both traditional and neural ones. For traditional codecs, we choose VVC and AVS3 because they are two state-of-the-arts. Their reference softwares, VTM-18.0 and HPM-15.1, are used for the compression. It is worth mentioning that VTM is also used as the inner codec in the VCM coding standard. To produce even more differences, we increase the internal bit depth to 10 for VVC (as a comparison, both HEVC and AVS3 are using the 8-bit compression configuration). The same QPs for HEVC are still used for VVC because they share the same QP ranges, whereas for AVS3, the selected QPs become 11, 16, 21, 24, 27, 30, 32, 34, 36, 37, . . . , 63. And each  $q_b$  for the corresponding  $T_{SMR}$  in  $\mathbb{T}_{SMR}$  is re-determined for each codec. Furthermore, the evaluation is also carried out on the test dataset annotated by the v2 machine library for *cls*, which challenges the SMR prediction models even more rigorously because they are still trained on HEVC-compressed v1 train dataset.

Results on VVC- and AVS3-compressed test datasets are presented in TABLE 5 (5-8th column) and 6 (5-6th column). Several facts can be concluded from these experiments: (1) The MAEs of predicted and actual SMRs all increase when solving unseen codecs for both *cls* and *det*. And the SMR predictions become even more inaccurate on v2 machine library for *cls*. However, the prediction performance remains acceptable. (2) SMR difference-based models can no longer always behave better than baseline models. For *cls*, using SMR difference-based models to predict SMRs annotated by the v2 machine library causes more errors than baseline models. For *det*, baseline models beat SMR difference-based models in predicting all types of SMR. The reason is that SMR difference-based models are trained with more HEVC-compressed images and are more familiar with HEVC distortions. (3) Using ground truth SMRs to guide QP selection for these unseen codecs achieves impressive and comparable coding gains for machines with HEVC. Using predicted SMRs also improves the coding performance consistently across different tasks, codecs, and machine library versions (for *cls*), which proves the strong generalizability of proposed SMR models. More importantly, as two of the most recent and advanced traditional compression framework, VVC and AVS3 significantly outperform HEVC in coding efficiency [104], yet our SMR models can help them further save a considerable amount of bits for machines. Therefore, SMR can be a feasible solution for optimizing currently-used codecs to achieve better coding efficiency and machine vision task performance without taking the risk and cost of replacing them.

As neural codecs are attracting more and more attention nowadays, we select two representative methods [102], [103] to further evaluate the generalizability of our SMR models, where [102] is a well-known baseline and [103] is the state-of-the-art. It should be mentioned that these neural codecs have much fewer operation points for modifying the compression quality than traditional codecs (there are only six "QPs" for each codec). Moreover, SMRs are more closed among different QPs on neural codecs (e.g. SMR-top1 ranges from 0.69 to 0.83 considering all six QPs). Hence, we decide to select  $T_{SMR}$  directly based on the QP-SMR distribution of these codecs for the evaluation. For SMR-top1,  $\mathbb{T}_{SMR} = [0.69 : 0.84 : 0.03]$ . For SMR-top5,  $\mathbb{T}_{SMR} = [0.90, 0.92, 0.94, 0.96, 0.97, 0.98]$ . For *det*,  $\mathbb{T}_{SMR} = [0.70, 0.80, 0.85, 0.90, 0.95, 0.98]$  when  $(T_{IOU}, T_S) = (0.5, 0.75)$ ,  $\mathbb{T}_{SMR} = [0.80, 0.88, 0.94, 0.96, 0.98]$  when  $(T_{IOU}, T_S) = (0.6, 0.6)$ . We don't evaluate coding performance when  $(T_{IOU}, T_S) = (0.5, 0.5)$  because SMR values are extremely closed to 0.99/1.0 at 4 of all 6 QPs, leaving almost no space for optimization.

TABLE 5 (9-12th column) and 6 (7-8th column) presents the prediction errors and coding efficiency increasements of the proposed SMR models (which remain being trained on HEVC-compressed v1 training dataset) on neural codecs. It can be observed that the MAE increases noticeably for *cls*, particularly for SMR-top1. This is because the SMR-top1 of images compressed with small QPs by neural codecs is substantially lower than those compressed by traditional codecs, even though their subjective quality is quite closed to the original images, indicating that the neural codec optimized for HVS may not be adaptive to MVS. For

*det*, however, the MAEs are decreased, because (i) images compressed with small QPs have high SMRs as expected at this time and (ii) SMR models excel in predicting SMR for high-quality images. With regard to coding performance improvement, for both tasks and all types of SMR, the theoretically optimal coding gains brought by applying ground truth SMRs are limited due to the fact that QP-SMR distributions are more balanced. Along with the existence of wrong SMR predictions, we can only achieve smaller coding gains on neural codecs than traditional ones. On the other hand, the SMR difference-based models almost outperform baseline models in all test conditions, and SMR models still generalize well on v2 dataset for *cls*. In conclusion, the proposed SMR models have an acceptable level of generalizability on neural codecs. We can expect that re-training these models to adapt to neural codec-produced distortions can improve their performance. Furthermore, SMR models should benefit from more operation points for the compression as well as more imbalanced SMR distributions.

## 7.6 Generalize to other datasets

We also evaluate the capability and generalizability of the proposed SMR models on other datasets than COCO. Two datasets are used for this experiment, which are the test2007 dataset of PASCAL VOC [105] and the TVD dataset [106]. They contain 13315 and 1098 valid object images, respectively. It is worth mentioning that (i) most object categories of VOC are also included in COCO except "sofa", thereby the semantics of images on VOC and COCO differ slightly, and (ii) TVD is a test dataset for the common test conditions of the emerging MPEG VCM standard. To produce more variables, we encode VOC with HEVC and TVD with VVC, and we also test the models on v1- and v2-annotated datasets separately. The SMR prediction errors and coding gains for *cls* are shown in TABLE 5 (last 4 columns). According to the results, again, all SMR models bring significant coding efficiency improvements, and SMR difference-based models are preferred over baseline models, which remain consistent with previous results on other traditional codecs-encoded COCO dataset. There is only one interesting outlier, i.e. SMR-top5 on HEVC-encoded VOC dataset, as the optimal BD-rate savings are noticeably smaller than other codec-dataset combinations. This means that the SMR distributions of two datasets can have some differences. Nevertheless, the generalizability of the proposed SMR models to any other data domain can be convinced considering all performed experiments.

## 8 CONCLUSION

In this paper, we propose a novel concept, Satisfied Machine Ratio (SMR), for video coding for machines. SMR statistically measures the quality of compressed images and videos for machines by modeling general machine perception characteristics. Targeting the image classification and object detection task, we build two machine libraries with up to 72 and 98 representative machine subjects to study the general MVS behavior and create a large-scale SMR dataset with over 27 million images to facilitate SMR studies. Furthermore, we propose an SMR model based on

the correlation between deep features difference and SMR, which can predict the SMR of any compressed image. To leverage all labeled data and improve prediction accuracy, we propose another SMR model based on SMR difference between a pair of images in different compression quality levels. Extensive experiments demonstrate the effectiveness of the proposed SMR models, revealing significant compression performance improvements for machines. And the SMR models generalize well to unseen machines, traditional and neural codecs, and other datasets. We believe that SMR enables the perceptual coding for machines and advances VCM from specificity to generality. The idea and statistical method of considering general machines instead of single specific machine can also benefit other related research areas.

## ACKNOWLEDGMENTS

This work was supported in part by the National Natural Science Foundation of China under grant 62072008 and U20A20184, and the High Performance Computing Platform of Peking University, which are gratefully acknowledged.

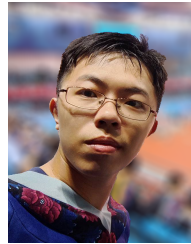
## REFERENCES

- [1] A. Krizhevsky, I. Sutskever, and G. E. Hinton, "Imagenet classification with deep convolutional neural networks," *Advances in neural information processing systems*, vol. 25, 2012.
- [2] K. Simonyan and A. Zisserman, "Very deep convolutional networks for large-scale image recognition," *arXiv preprint arXiv:1409.1556*, 2014.
- [3] Y. LeCun, Y. Bengio, and G. Hinton, "Deep learning," *nature*, vol. 521, no. 7553, pp. 436–444, 2015.
- [4] K. He, X. Zhang, S. Ren, and J. Sun, "Deep residual learning for image recognition," in *Proceedings of the IEEE conference on computer vision and pattern recognition*, 2016, pp. 770–778.
- [5] G. Huang, Z. Liu, L. Van Der Maaten, and K. Q. Weinberger, "Densely connected convolutional networks," in *Proceedings of the IEEE conference on computer vision and pattern recognition*, 2017, pp. 4700–4708.
- [6] G. Hinton, O. Vinyals, and J. Dean, "Distilling the knowledge in a neural network," *arXiv preprint arXiv:1503.02531*, 2015.
- [7] B. Zoph and Q. V. Le, "Neural architecture search with reinforcement learning," *arXiv preprint arXiv:1611.01578*, 2016.
- [8] M. Tan, B. Chen, R. Pang, V. Vasudevan, M. Sandler, A. Howard, and Q. V. Le, "Mnasnet: Platform-aware neural architecture search for mobile," in *Proceedings of the IEEE/CVF Conference on Computer Vision and Pattern Recognition*, 2019, pp. 2820–2828.
- [9] A. Dosovitskiy, L. Beyer, A. Kolesnikov, D. Weissenborn, X. Zhai, T. Unterthiner, M. Dehghani, M. Minderer, G. Heigold, S. Gelly *et al.*, "An image is worth 16x16 words: Transformers for image recognition at scale," *arXiv preprint arXiv:2010.11929*, 2020.
- [10] Z. Liu, Y. Lin, Y. Cao, H. Hu, Y. Wei, Z. Zhang, S. Lin, and B. Guo, "Swin transformer: Hierarchical vision transformer using shifted windows," in *Proceedings of the IEEE/CVF International Conference on Computer Vision*, 2021, pp. 10 012–10 022.
- [11] T. Chen, S. Kornblith, M. Norouzi, and G. Hinton, "A simple framework for contrastive learning of visual representations," in *International conference on machine learning*. PMLR, 2020, pp. 1597–1607.
- [12] K. He, X. Chen, S. Xie, Y. Li, P. Dollár, and R. Girshick, "Masked autoencoders are scalable vision learners," in *Proceedings of the IEEE/CVF conference on computer vision and pattern recognition*, 2022, pp. 16 000–16 009.
- [13] K. He, X. Zhang, S. Ren, and J. Sun, "Delving deep into rectifiers: Surpassing human-level performance on imagenet classification," in *Proceedings of the IEEE international conference on computer vision*, 2015, pp. 1026–1034.
- [14] D. Silver, A. Huang, C. J. Maddison, A. Guez, L. Sifre, G. Van Den Driessche, J. Schrittwieser, I. Antonoglou, V. Panneershelvam, M. Lanctot *et al.*, "Mastering the game of go with deep neural networks and tree search," *nature*, vol. 529, no. 7587, pp. 484–489, 2016.
- [15] J. Deng, W. Dong, R. Socher, L.-J. Li, K. Li, and L. Fei-Fei, "Imagenet: A large-scale hierarchical image database," in *2009 IEEE conference on computer vision and pattern recognition*. Ieee, 2009, pp. 248–255.
- [16] T.-Y. Lin, M. Maire, S. Belongie, J. Hays, P. Perona, D. Ramanan, P. Dollár, and C. L. Zitnick, "Microsoft coco: Common objects in context," in *European conference on computer vision*. Springer, 2014, pp. 740–755.
- [17] S. Dodge and L. Karam, "Understanding how image quality affects deep neural networks," in *2016 eighth international conference on quality of multimedia experience (QoMEX)*. IEEE, 2016, pp. 1–6.
- [18] R. Geirhos, C. R. Temme, J. Rauber, H. H. Schütt, M. Bethge, and F. A. Wichmann, "Generalisation in humans and deep neural networks," *Advances in neural information processing systems*, vol. 31, 2018.
- [19] S. Ma, X. Zhang, S. Wang, X. Zhang, C. Jia, and S. Wang, "Joint feature and texture coding: Toward smart video representation via front-end intelligence," *IEEE Transactions on Circuits and Systems for Video Technology*, vol. 29, no. 10, pp. 3095–3105, 2018.
- [20] M. Aqqa, P. Mantini, and S. K. Shah, "Understanding how video quality affects object detection algorithms." in *VISIGRAPP (5: VISAPP)*, 2019, pp. 96–104.
- [21] Q. Zhang, S. Wang, X. Zhang, S. Ma, and W. Gao, "Just recognizable distortion for machine vision oriented image and video coding," *International Journal of Computer Vision*, vol. 129, no. 10, pp. 2889–2906, 2021.
- [22] G. K. Wallace, "The jpeg still picture compression standard," *Communications of the ACM*, vol. 34, no. 4, pp. 30–44, 1991.
- [23] T. Wiegand, G. J. Sullivan, G. Bjontegaard, and A. Luthra, "Overview of the h. 264/avc video coding standard," *IEEE Transactions on circuits and systems for video technology*, vol. 13, no. 7, pp. 560–576, 2003.
- [24] G. J. Sullivan, J.-R. Ohm, W.-J. Han, and T. Wiegand, "Overview of the high efficiency video coding (hevc) standard," *IEEE Transactions on circuits and systems for video technology*, vol. 22, no. 12, pp. 1649–1668, 2012.
- [25] B. Bross, Y.-K. Wang, Y. Ye, S. Liu, J. Chen, G. J. Sullivan, and J.-R. Ohm, "Overview of the versatile video coding (vvc) standard and its applications," *IEEE Transactions on Circuits and Systems for Video Technology*, vol. 31, no. 10, pp. 3736–3764, 2021.
- [26] J. Han, B. Li, D. Mukherjee, C.-H. Chiang, A. Grange, C. Chen, H. Su, S. Parker, S. Deng, U. Joshi *et al.*, "A technical overview of av1," *Proceedings of the IEEE*, vol. 109, no. 9, pp. 1435–1462, 2021.
- [27] J. Zhang, C. Jia, M. Lei, S. Wang, S. Ma, and W. Gao, "Recent development of avs video coding standard: Avs3," in *2019 picture coding symposium (PCS)*. IEEE, 2019, pp. 1–5.
- [28] S. Ma, X. Zhang, C. Jia, Z. Zhao, S. Wang, and S. Wang, "Image and video compression with neural networks: A review," *IEEE Transactions on Circuits and Systems for Video Technology*, vol. 30, no. 6, pp. 1683–1698, 2019.
- [29] Y. Hu, W. Yang, Z. Ma, and J. Liu, "Learning end-to-end lossy image compression: A benchmark," *IEEE Transactions on Pattern Analysis and Machine Intelligence*, 2021.
- [30] D. Liu, D. Wang, and H. Li, "Recognizable or not: Towards image semantic quality assessment for compression," *Sensing and Imaging*, vol. 18, no. 1, pp. 1–20, 2017.
- [31] X. Li, J. Shi, and Z. Chen, "Task-driven semantic coding via reinforcement learning," *IEEE Transactions on Image Processing*, vol. 30, pp. 6307–6320, 2021.
- [32] X. Zhang, S. Ma, S. Wang, X. Zhang, H. Sun, and W. Gao, "A joint compression scheme of video feature descriptors and visual content," *IEEE Transactions on Image Processing*, vol. 26, no. 2, pp. 633–647, 2016.
- [33] Q. Zhang, S. Wang, and S. Ma, "A novel visual analysis oriented rate control scheme for hevc," in *2020 IEEE International Conference on Visual Communications and Image Processing (VCIP)*. IEEE, 2020, pp. 491–494.
- [34] K. Fischer, F. Brand, C. Herglotz, and A. Kaup, "Video coding for machines with feature-based rate-distortion optimization," in *2020 IEEE 22nd International Workshop on Multimedia Signal Processing (MMSP)*. IEEE, 2020, pp. 1–6.

- [35] L. Galteri, M. Bertini, L. Seidenari, and A. Del Bimbo, "Video compression for object detection algorithms," in *2018 24th International Conference on Pattern Recognition (ICPR)*. IEEE, 2018, pp. 3007–3012.
- [36] H. Choi and I. V. Bajic, "High efficiency compression for object detection," in *2018 IEEE International Conference on Acoustics, Speech and Signal Processing (ICASSP)*. IEEE, 2018, pp. 1792–1796.
- [37] Z. Huang, C. Jia, S. Wang, and S. Ma, "Visual analysis motivated rate-distortion model for image coding," in *2021 IEEE International Conference on Multimedia and Expo (ICME)*. IEEE, 2021, pp. 1–6.
- [38] S. Luo, Y. Yang, Y. Yin, C. Shen, Y. Zhao, and M. Song, "DeepSic: Deep semantic image compression," in *International Conference on Neural Information Processing*. Springer, 2018, pp. 96–106.
- [39] R. Torfason, F. Mentzer, E. Agustsson, M. Tschannen, R. Timofte, and L. Van Gool, "Towards image understanding from deep compression without decoding," *arXiv preprint arXiv:1803.06131*, 2018.
- [40] Y. Bai, X. Yang, X. Liu, J. Jiang, Y. Wang, X. Ji, and W. Gao, "Towards end-to-end image compression and analysis with transformers," in *Proceedings of the AAAI Conference on Artificial Intelligence*, vol. 36, 2022, pp. 104–112.
- [41] R. Feng, X. Jin, Z. Guo, R. Feng, Y. Gao, T. He, Z. Zhang, S. Sun, and Z. Chen, "Image coding for machines with omnipotent feature learning," in *European Conference on Computer Vision*. Springer, 2022, pp. 510–528.
- [42] C. Hollmann, S. Liu, C. Rosewarne, and Y. Zhang, "Use cases and requirements for Video Coding for Machines," MPEG Output Document ISO/IEC JTC1/SC29/WG2/N190, 2022.
- [43] W. Gao, S. Liu, X. Xu, M. Rafie, Y. Zhang, and I. Curcio, "Recent standard development activities on video coding for machines," *arXiv preprint arXiv:2105.12653*, 2021.
- [44] S. Liu, H. Zhang, and C. Rosewarne, "Common test conditions for video coding for machines," MPEG Output Document ISO/IEC JTC1/SC29/WG4/N332, 2023.
- [45] Y. Zhang, L. Zhu, G. Jiang, S. Kwong, and C.-C. J. Kuo, "A survey on perceptually optimized video coding," *ACM Computing Surveys*, vol. 55, no. 12, pp. 1–37, 2023.
- [46] N. Jayant, J. Johnston, and R. Safranek, "Signal compression based on models of human perception," *Proceedings of the IEEE*, vol. 81, no. 10, pp. 1385–1422, 1993.
- [47] C.-H. Chou and Y.-C. Li, "A perceptually tuned subband image coder based on the measure of just-noticeable-distortion profile," *IEEE Transactions on circuits and systems for video technology*, vol. 5, no. 6, pp. 467–476, 1995.
- [48] X. Yang, W. Ling, Z. Lu, E. P. Ong, and S. Yao, "Just noticeable distortion model and its applications in video coding," *Signal processing: Image communication*, vol. 20, no. 7, pp. 662–680, 2005.
- [49] H. Liu, Y. Zhang, H. Zhang, C. Fan, S. Kwong, C.-C. J. Kuo, and X. Fan, "Deep learning-based picture-wise just noticeable distortion prediction model for image compression," *IEEE Transactions on Image Processing*, vol. 29, pp. 641–656, 2019.
- [50] X. Shen, Z. Ni, W. Yang, X. Zhang, S. Wang, and S. Kwong, "Just noticeable distortion profile inference: A patch-level structural visibility learning approach," *IEEE Transactions on Image Processing*, vol. 30, pp. 26–38, 2020.
- [51] Q. Jiang, Z. Liu, S. Wang, F. Shao, and W. Lin, "Toward top-down just noticeable difference estimation of natural images," *IEEE Transactions on Image Processing*, vol. 31, pp. 3697–3712, 2022.
- [52] H. Wang, I. Katsavounidis, J. Zhou, J. Park, S. Lei, X. Zhou, M.-O. Pun, X. Jin, R. Wang, X. Wang *et al.*, "Videose: A large-scale compressed video quality dataset based on jnd measurement," *Journal of Visual Communication and Image Representation*, vol. 46, pp. 292–302, 2017.
- [53] C. Fan, H. Lin, V. Hosu, Y. Zhang, Q. Jiang, R. Hamzaoui, and D. Saupe, "Sur-net: Predicting the satisfied user ratio curve for image compression with deep learning," in *2019 eleventh international conference on quality of multimedia experience (QoMEX)*. IEEE, 2019, pp. 1–6.
- [54] X. Zhang, C. Yang, H. Wang, W. Xu, and C.-C. J. Kuo, "Satisfied-user-ratio modeling for compressed video," *IEEE Transactions on Image Processing*, vol. 29, pp. 3777–3789, 2020.
- [55] Y. Zhang, H. Liu, Y. Yang, X. Fan, S. Kwong, and C. J. Kuo, "Deep learning based just noticeable difference and perceptual quality prediction models for compressed video," *IEEE Transactions on Circuits and Systems for Video Technology*, vol. 32, no. 3, pp. 1197–1212, 2021.
- [56] J. Jin, X. Zhang, X. Fu, H. Zhang, W. Lin, J. Lou, and Y. Zhao, "Just noticeable difference for deep machine vision," *IEEE Transactions on Circuits and Systems for Video Technology*, 2021.
- [57] W. Yang, H. Huang, Y. Hu, L.-Y. Duan, and J. Liu, "Video coding for machine: Compact visual representation compression for intelligent collaborative analytics," *arXiv preprint arXiv:2110.09241*, 2021.
- [58] J. Shi and Z. Chen, "Reinforced bit allocation under task-driven semantic distortion metrics," in *2020 IEEE international symposium on circuits and systems (ISCAS)*. IEEE, 2020, pp. 1–5.
- [59] Y. Li, C. Jia, S. Wang, X. Zhang, S. Wang, S. Ma, and W. Gao, "Joint rate-distortion optimization for simultaneous texture and deep feature compression of facial images," in *2018 IEEE fourth international conference on multimedia big data (BigMM)*. IEEE, 2018, pp. 1–5.
- [60] F. Codevilla, J. G. Simard, R. Goroshin, and C. Pal, "Learned image compression for machine perception," *arXiv preprint arXiv:2111.02249*, 2021.
- [61] L. D. Chamain, F. Racapé, J. Bégaint, A. Pushparaja, and S. Feltman, "End-to-end optimized image compression for multiple machine tasks," *arXiv preprint arXiv:2103.04178*, 2021.
- [62] Y. Dubois, B. Bloem-Reddy, K. Ullrich, and C. J. Maddison, "Lossy compression for lossless prediction," *Advances in Neural Information Processing Systems*, vol. 34, 2021.
- [63] M. Akbari, J. Liang, and J. Han, "Dsslic: Deep semantic segmentation-based layered image compression," in *ICASSP 2019-2019 IEEE International Conference on Acoustics, Speech and Signal Processing (ICASSP)*. IEEE, 2019, pp. 2042–2046.
- [64] Y. Hu, S. Yang, W. Yang, L.-Y. Duan, and J. Liu, "Towards coding for human and machine vision: A scalable image coding approach," in *2020 IEEE International Conference on Multimedia and Expo (ICME)*. IEEE, 2020, pp. 1–6.
- [65] S. Yang, Y. Hu, W. Yang, L.-Y. Duan, and J. Liu, "Towards coding for human and machine vision: Scalable face image coding," *IEEE Transactions on Multimedia*, vol. 23, pp. 2957–2971, 2021.
- [66] J. Chang, Z. Zhao, C. Jia, S. Wang, L. Yang, Q. Mao, J. Zhang, and S. Ma, "Conceptual compression via deep structure and texture synthesis," *IEEE Transactions on Image Processing*, vol. 31, pp. 2809–2823, 2022.
- [67] J. Chang, J. Zhang, J. Li, S. Wang, Q. Mao, C. Jia, S. Ma, and W. Gao, "Semantic-aware visual decomposition for image coding," *International Journal of Computer Vision*, pp. 1–23, 2023.
- [68] S. Wang, S. Wang, X. Zhang, S. Wang, S. Ma, and W. Gao, "Scalable facial image compression with deep feature reconstruction," in *2019 IEEE International Conference on Image Processing (ICIP)*. IEEE, 2019, pp. 2691–2695.
- [69] S. Wang, S. Wang, W. Yang, X. Zhang, S. Wang, S. Ma, and W. Gao, "Towards analysis-friendly face representation with scalable feature and texture compression," *IEEE Transactions on Multimedia*, 2021.
- [70] N. Yan, D. Liu, H. Li, and F. Wu, "Semantically scalable image coding with compression of feature maps," in *2020 IEEE International Conference on Image Processing (ICIP)*. IEEE, 2020, pp. 3114–3118.
- [71] N. Yan, C. Gao, D. Liu, H. Li, L. Li, and F. Wu, "Sssic: Semantics-to-signal scalable image coding with learned structural representations," *IEEE Transactions on Image Processing*, vol. 30, pp. 8939–8954, 2021.
- [72] K. Liu, D. Liu, L. Li, N. Yan, and H. Li, "Semantics-to-signal scalable image compression with learned revertible representations," *International Journal of Computer Vision*, vol. 129, no. 9, pp. 2605–2621, 2021.
- [73] H. Tu, L. Li, W. Zhou, and H. Li, "Semantic scalable image compression with cross-layer priors," in *Proceedings of the 29th ACM International Conference on Multimedia*, 2021, pp. 4044–4052.
- [74] H. Choi and I. V. Bajic, "Latent-space scalability for multi-task collaborative intelligence," in *2021 IEEE International Conference on Image Processing (ICIP)*. IEEE, 2021, pp. 3562–3566.
- [75] T. He, S. Sun, Z. Guo, and Z. Chen, "Beyond coding: Detection-driven image compression with semantically structured bit-stream," in *2019 Picture Coding Symposium (PCS)*. IEEE, 2019, pp. 1–5.
- [76] S. Sun, T. He, and Z. Chen, "Semantic structured image coding framework for multiple intelligent applications," *IEEE Transactions on Circuits and Systems for Video Technology*, vol. 31, no. 9, pp. 3631–3642, 2020.



- [77] X. Jin, R. Feng, S. Sun, R. Feng, T. He, and Z. Chen, "Semantically video coding: Instill static-dynamic clues into structured bitstream for ai tasks," *arXiv preprint arXiv:2201.10162*, 2022.
- [78] H. Choi and I. V. Bajić, "Scalable image coding for humans and machines," *IEEE Transactions on Image Processing*, vol. 31, pp. 2739–2754, 2022.
- [79] T. Sikora, "The mpeg-7 visual standard for content description-an overview," *IEEE Transactions on circuits and systems for video technology*, vol. 11, no. 6, pp. 696–702, 2001.
- [80] L.-Y. Duan, V. Chandrasekhar, J. Chen, J. Lin, Z. Wang, T. Huang, B. Girod, and W. Gao, "Overview of the mpeg-cdvs standard," *IEEE Transactions on Image Processing*, vol. 25, no. 1, pp. 179–194, 2015.
- [81] L.-Y. Duan, Y. Lou, Y. Bai, T. Huang, W. Gao, V. Chandrasekhar, J. Lin, S. Wang, and A. C. Kot, "Compact descriptors for video analysis: The emerging mpeg standard," *IEEE MultiMedia*, vol. 26, no. 2, pp. 44–54, 2018.
- [82] W. Gao, S. Ma, L. Duan, Y. Tian, P. Xing, Y. Wang, S. Wang, H. Jia, and T. Huang, "Digital retina: A way to make the city brain more efficient by visual coding," *IEEE Transactions on Circuits and Systems for Video Technology*, vol. 31, no. 11, pp. 4147–4161, 2021.
- [83] L. Jin, J. Y. Lin, S. Hu, H. Wang, P. Wang, I. Katsavounidis, A. Aaron, and C.-C. J. Kuo, "Statistical study on perceived jpeg image quality via mcl-jci dataset construction and analysis," *Electronic Imaging*, vol. 2016, no. 13, pp. 1–9, 2016.
- [84] H. Wang, W. Gan, S. Hu, J. Y. Lin, L. Jin, L. Song, P. Wang, I. Katsavounidis, A. Aaron, and C.-C. J. Kuo, "Mcl-jcv: a jnd-based h. 264/avc video quality assessment dataset," in *2016 IEEE international conference on image processing (ICIP)*. IEEE, 2016, pp. 1509–1513.
- [85] W. Lin and G. Ghinea, "Progress and opportunities in modelling just-noticeable difference (jnd) for multimedia," *IEEE Transactions on Multimedia*, vol. 24, pp. 3706–3721, 2021.
- [86] Q. Huang, H. Wang, S. C. Lim, H. Y. Kim, S. Y. Jeong, and C.-C. J. Kuo, "Measure and prediction of hevcc perceptually lossy/lossless boundary qp values," in *2017 data compression conference (DCC)*. IEEE, 2017, pp. 42–51.
- [87] T. Tian, H. Wang, L. Zuo, C.-C. J. Kuo, and S. Kwong, "Just noticeable difference level prediction for perceptual image compression," *IEEE Transactions on Broadcasting*, vol. 66, no. 3, pp. 690–700, 2020.
- [88] H. Wang, I. Katsavounidis, Q. Huang, X. Zhou, and C.-C. J. Kuo, "Prediction of satisfied user ratio for compressed video," in *2018 IEEE international conference on acoustics, speech and signal processing (ICASSP)*. IEEE, 2018, pp. 6747–6751.
- [89] H. Wang, X. Zhang, C. Yang, and C.-C. J. Kuo, "Analysis and prediction of jnd-based video quality model," in *2018 picture coding symposium (PCS)*. IEEE, 2018, pp. 278–282.
- [90] H. Lin, V. Hosu, C. Fan, Y. Zhang, Y. Mu, R. Hamzaoui, and D. Saupe, "Sur-featnet: Predicting the satisfied user ratio curve for image compression with deep feature learning," *Quality and User Experience*, vol. 5, no. 1, pp. 1–23, 2020.
- [91] S. Xie, R. Girshick, P. Dollár, Z. Tu, and K. He, "Aggregated residual transformations for deep neural networks," in *Proceedings of the IEEE conference on computer vision and pattern recognition*, 2017, pp. 1492–1500.
- [92] A. Howard, M. Sandler, G. Chu, L.-C. Chen, B. Chen, M. Tan, W. Wang, Y. Zhu, R. Pang, V. Vasudevan *et al.*, "Searching for mobilenetv3," in *Proceedings of the IEEE/CVF international conference on computer vision*, 2019, pp. 1314–1324.
- [93] M. Tan and Q. Le, "Efficientnet: Rethinking model scaling for convolutional neural networks," in *International conference on machine learning*. PMLR, 2019, pp. 6105–6114.
- [94] Z. Liu, H. Mao, C.-Y. Wu, C. Feichtenhofer, T. Darrell, and S. Xie, "A convnet for the 2020s," in *Proceedings of the IEEE/CVF Conference on Computer Vision and Pattern Recognition*, 2022, pp. 11976–11986.
- [95] A. Paszke, S. Gross, F. Massa, A. Lerer, J. Bradbury, G. Chanan, T. Killeen, Z. Lin, N. Gimelshein, L. Antiga *et al.*, "Pytorch: An imperative style, high-performance deep learning library," *Advances in neural information processing systems*, vol. 32, 2019.
- [96] K. Fischer, M. Hofbauer, C. Kuhn, E. Steinbach, and A. Kaup, "Evaluation of video coding for machines without ground truth," in *ICASSP 2022-2022 IEEE International Conference on Acoustics, Speech and Signal Processing (ICASSP)*. IEEE, 2022, pp. 1616–1620.
- [97] PyTorch/Torchvision, "Models and pre-trained weights," <https://pytorch.org/vision/stable/models.html#classification>, 2023.
- [98] MMDetection, "Benchmark and Model Zoo," [https://mmdetection.readthedocs.io/en/latest/model\\_zoo.html#baselines](https://mmdetection.readthedocs.io/en/latest/model_zoo.html#baselines), 2023.
- [99] K. Chen, J. Wang, J. Pang, Y. Cao, Y. Xiong, X. Li, S. Sun, W. Feng, Z. Liu, J. Xu *et al.*, "Mmdetection: Open mmlab detection toolbox and benchmark," *arXiv preprint arXiv:1906.07155*, 2019.
- [100] H. Lin, G. Chen, M. Jenadeleh, V. Hosu, U.-D. Reips, R. Hamzaoui, and D. Saupe, "Large-scale crowdsourced subjective assessment of picturewise just noticeable difference," *IEEE transactions on circuits and systems for video technology*, 2022.
- [101] G. Bjontegaard, "Calculation of average psnr differences between rd-curves," *VCEG-M33*, 2001.
- [102] Z. Cheng, H. Sun, M. Takeuchi, and J. Katto, "Learned image compression with discretized gaussian mixture likelihoods and attention modules," in *Proceedings of the IEEE/CVF conference on computer vision and pattern recognition*, 2020, pp. 7939–7948.
- [103] J. Liu, H. Sun, and J. Katto, "Learned image compression with mixed transformer-cnn architectures," in *Proceedings of the IEEE/CVF Conference on Computer Vision and Pattern Recognition*, 2023, pp. 14388–14397.
- [104] X. Zhao, S. Liu, L. Zhao, X. Xu, B. Zhu, and X. Li, "A comparative study of hevcc, vvc, vp9, av1 and avs3 video codecs," in *Applications of Digital Image Processing XLIII*, vol. 11510. SPIE, 2020, pp. 192–200.
- [105] M. Everingham, L. Van Gool, C. K. Williams, J. Winn, and A. Zisserman, "The pascal visual object classes (voc) challenge," *International journal of computer vision*, vol. 88, pp. 303–338, 2010.
- [106] W. Gao, X. Xu, M. Qin, and S. Liu, "An open dataset for video coding for machines standardization," in *2022 IEEE International Conference on Image Processing (ICIP)*. IEEE, 2022, pp. 4008–4012.



**Qi Zhang** (Student Member, IEEE) received the B.S. degree in software engineering from Hefei University of Technology, Hefei, China, in 2017, and the M.S. degree in computer application technology from Peking University, Beijing, China, in 2020. He is currently pursuing the Ph.D. degree with the Department of Computer Science, Peking University, Beijing. His research interests include video coding for both humans and machines, immersive video technology, and virtual reality.



**Shanshe Wang** (Member, IEEE) received the B.S. degree from the Department of Mathematics, Heilongjiang University, Harbin, China, in 2004, the M.S. degree in computer software and theory from Northeast Petroleum University, Daqing, China, in 2010, and the Ph.D. degree in computer science from the Harbin Institute of Technology, Harbin, China, in 2014. He held a post-doctoral position with Peking University from 2016 to 2018. He joined the School of Electronics Engineering and Computer Science, Institute of Digital Media, Peking University, Beijing, where he is currently a Research Associate Professor. His current research interests include video compression and video quality assessment.



**Xinfeng Zhang** (Senior Member, IEEE) received the B.S. degree in computer science from the Hebei University of Technology, Tianjin, China, in 2007, and the Ph.D. degree in computer science from the Institute of Computing Technology, Chinese Academy of Sciences, Beijing, China, in 2014. From 2014 to 2017, he was a Research Fellow with the Rapid-Rich Object Search Laboratory, Nanyang Technological University, Singapore. From October 2017 to October 2018, he was a Postdoctoral Fellow with the School of

Electrical Engineering System, University of Southern California, Los Angeles, CA, USA. From December 2018 to August 2019, he was a Research Fellow with the Department of Computer Science, City University of Hong Kong. He is currently an Associate Professor with the School of Computer Science and Technology, University of Chinese Academy of Sciences. He has authored more than 160 refereed journals/conference papers. He received the Best Paper Award of IEEE Multimedia 2018, the Best Paper Award at the 2017 Pacific-Rim Conference on Multimedia (PCM), and the Best Student Paper Award in IEEE International Conference on Image Processing 2018. His research interests include video compression and processing, image/video quality assessment, and 3D point cloud processing.



**Siwei Ma** (Senior Member, IEEE) received the B.S. degree from Shandong Normal University, Jinan, China, in 1999, and the Ph.D. degree in computer science from the Institute of Computing Technology, Chinese Academy of Sciences, Beijing, China, in 2005. He held a postdoctoral position with the University of Southern California, Los Angeles, CA, USA, from 2005 to 2007. He joined the School of Electronics Engineering and Computer Science, Institute of Digital Media, Peking University, Beijing, where he is

currently a Professor. He has authored over 300 technical articles in refereed journals and proceedings in image and video coding, video processing, video streaming, and transmission. He served/serves as an Associate Editor for the IEEE Transactions on Circuits and Systems for Video Technology and the Journal of Visual Communication and Image Representation.



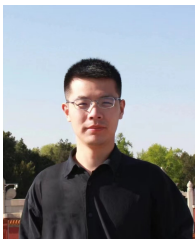
**Chuanmin Jia** (Member, IEEE) received the B.E. degree in computer science from the Beijing University of Posts and Telecommunications, Beijing, China, in 2015, and the Ph.D. degree in computer application technology from Peking University, Beijing, in 2020. He was a Visiting Student at New York University, USA, in 2018. He is currently an Assistant Professor with the Wangxuan Institute of Computer Technology, Peking University. His research interests include

video compression and multimedia signal processing. He received the Best Paper Award of PCM 2017, the Best Paper Award of IEEE Multimedia 2018, and the Best Student Paper Award of IEEE MIPR 2019.



**Wen Gao** (Fellow, IEEE) received the Ph.D. degree in electronics engineering from The University of Tokyo, Japan, in 1991. He is currently a Boya Chair Professor in computer science at Peking University. He is also the Director of the Peng Cheng Laboratory, Shenzhen. Before joining Peking University, he was a Professor with the Harbin Institute of Technology, from 1991 to 1995. From 1996 to 2006, he was a Professor with the Institute of Computing Technology, Chinese Academy of Sciences. He has published

extensively, including five books and over 1000 technical articles in refereed journals and conference proceedings in the areas of image processing, video coding and communication, computer vision, multimedia retrieval, multimodal interface, and bioinformatics. He served on the editorial boards for several journals, such as ACM CSUR, IEEE Transactions on Image Processing (TIP), IEEE Transactions on Circuits and Systems for Video Technology (TCSVT), and IEEE Transactions on Multimedia (TMM). He served on the advisory and technical committees for professional organizations. He was the Vice President of the National Natural Science Foundation (NSFC) of China, from 2013 to 2018, and the President of China Computer Federation (CCF), from 2016 to 2020. He is also the Deputy Director of China National Standardization Technical Committees. He is an Academician of the Chinese Academy of Engineering and a fellow of ACM. He chaired a number of international conferences, such as IEEE ICME 2007, ACM Multimedia 2009, and IEEE ISCAS 2013.



**Zhao Wang** (Member, IEEE) received the B.S. degree in software engineering from Fudan University in 2014, and the Ph.D. degree in computer science from Peking University in 2019. He previously worked at the DAMO Academy of Alibaba Group as an Algorithm Expert, and currently work at Peking University as an Engineer. His research interests include video compression, multi-modality vision coding and analysis. He has published more than 20 papers, and proposed more than 40 technical proposals to

JVET, MPEG and AVS standards. He received the Best Student Paper Award from IEEE ICIP 2018, and his doctoral thesis was awarded the Excellent Doctoral Dissertation of Peking University.